

Laser ablation ICP-MS on KCC microstructure – pilot study –

Climate Change Institute, Maine

June 8 – 19, 2015

Johanna Kerch*, Nicole Spaulding†, Pascal Bohleber*†

Version 1.5 of the report

September 4, 2015



*Institute of Environmental Physics, Heidelberg University, Germany

†Climate Change Institute, University of Maine, USA

Contents

Acknowledgements	3
Summary	3
1 Motivation	3
2 Hypotheses and questions	3
3 Objectives for the laboratory work	4
4 Laser parameter testing	6
5 KCC Samples	6
6 Measurement pattern	10
6.1 Grains	10
6.2 Variability lines	10
6.3 Mesh	12
7 Calibration	12
8 Methodological comments	12
9 Preliminary findings	13
9.1 Grain concentration gradients	13
9.1.1 Summary and conclusions	17
9.1.2 Open questions	23
9.2 Laser ICP-MS signal variability	23
9.3 Impurity mapping from mesh data	23
A Comparison between sections for each feature	24
A.1 Sodium	24
A.2 Iron	25
B Laser ablation traces	26
C Smoothed data for each grain	27
C.1 Sodium	27
C.2 Iron	36

Acknowledgements

We would like to thank Dr. Paul Mayewski, Director of the Climate Change Institute, and Sharon Sneed, LA-ICP-MS Lab manager, for the opportunity to conduct this pilot study at the Keck Laser Ice Facility. This research was supported by the Arcadia Fund of London (AC3450). J.K. was funded by the Studienstiftung des deutschen Volkes and acknowledges the support of her Ph.D. advisors Olaf Eisen and Ilka Weikusat.

Summary

In a two week pilot study at the Keck Laser Ice Facility at the Climate Change Institute in Orono, Maine laser ablation ICP-MS experiments were conducted on samples from four depths of the Alpine ice core KCC from Colle Gnifetti that were selected based on available fabric and microstructure data. Impurity fractions of sodium, iron and calcium were measured with respect to the visible microstructure on the ice sample surface.

The first assesement of the data suggests that sodium concentrations are increased in the grain boundaries regardless of ice core depth and grain properties, while iron concentrations show no pattern.

Although the results cannot be interpreted conclusively – due to the pilot character of the study – the potential of this technique for high resolution impurity measurements with regard to the local microstructure becomes evident and possible improvements for deeper studies could be identified.

1 Motivation

The presented pilot study addresses two issues:

Firstly, the signal obtained by laser ablation ICP-MS from ice is not fully understood to date, i.e. the respective contribution of impurities on inter- and intra-grain-scale has not been investigated so far. It is unclear if a microstructure-governed impurity signal could be modulating the climate-governed impurity signal (e.g. producing spikes on grain boundaries) in a significant way, thus complicating the interpretation.

Secondly, impurity data measured by continuous flow analysis represents a bulk signal of the melted ice without consideration for the original microstructure of the ice matrix.

From a fundamental point of view, the new method LA-ICPMS allows, for the first time, to do both: Obtain impurity profiles and afford spatial resolution high enough to investigate microstructural effects.

2 Hypotheses and questions

- Inhomogeneous impurity distributions develop with depth due to ongoing recrystallization processes and dragging/pinning effects. We expect to find a radial gradient, i.e. between grain boundary and grain interior towards the boundaries, which becomes stronger with depth. This might be different for different impurity species due to mobility and electronegativity differences. The differences might show in mean value comparison or variability changes (e.g. the number of peaks above the base line)
- Can the impurity stratigraphy – that is used for dating – be preserved in the deep part of the core if the mean grain size exceeds the layer thickness (Fig. 1)?

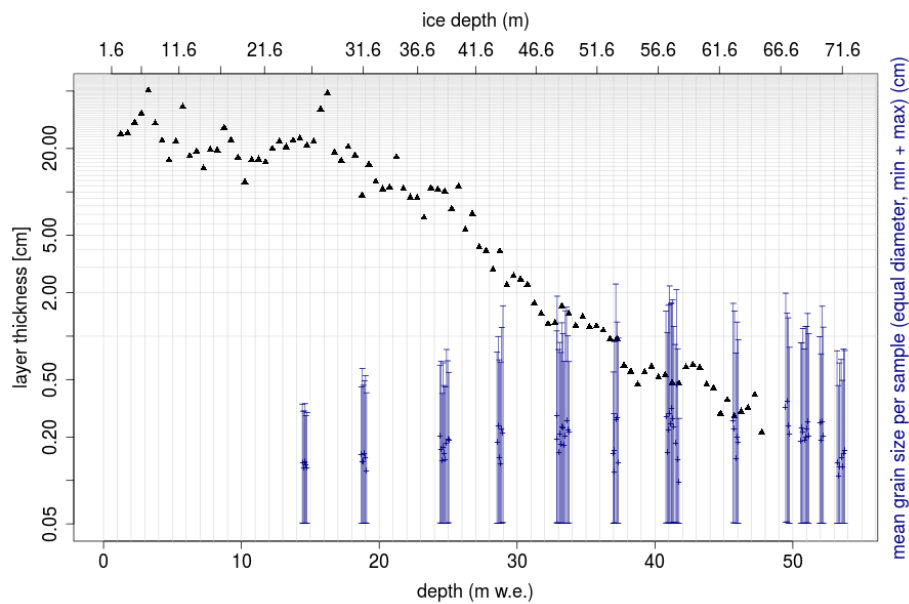


Figure 1: Layer thickness from dating (effective March 2015) and mean grain sizes (bars extend to minimum and maximum values per sample) from fabric measurements. Below 40 m ice depth crystals exceeding the layer thickness can be found regularly.

- As to now it is assumed that the low-frequency part of the laser signal corresponds to the CFA data i.e. the signal from the soluble portion of the total impurity content while the high-frequency part of the laser signal provides additional information but is only insufficiently understood, so far. In addition, instrument-based artifacts may bias the high frequency components, e.g. turbulent gas flow within the ablation chamber.
- Annual layer peaks, where present, are larger than peaks from grain boundaries or other microstructural evolved impurity accumulation.
- Grain size could be controlled by a maximum amount of impurities that can accumulate and be distributed in a given grain boundary network/vein volume. Higher overall impurity content would demand a larger volume, thus keeping grains small (suggestion F. Wilhelms).

3 Objectives for the laboratory work

- Measurements in different depths: shallow (below ice-firn-transition), intermediate and with exceptional characteristics, deep, close to bed rock (also exceptional)
- Measurements within layers of different microstructural characteristics within each depth, i.e. within a large (less oriented) grain section and a small grain section
- Measurements between grain boundaries and grain interiors, also triple junctions
- Measurements of signal variability dependent on microstructural characteristics

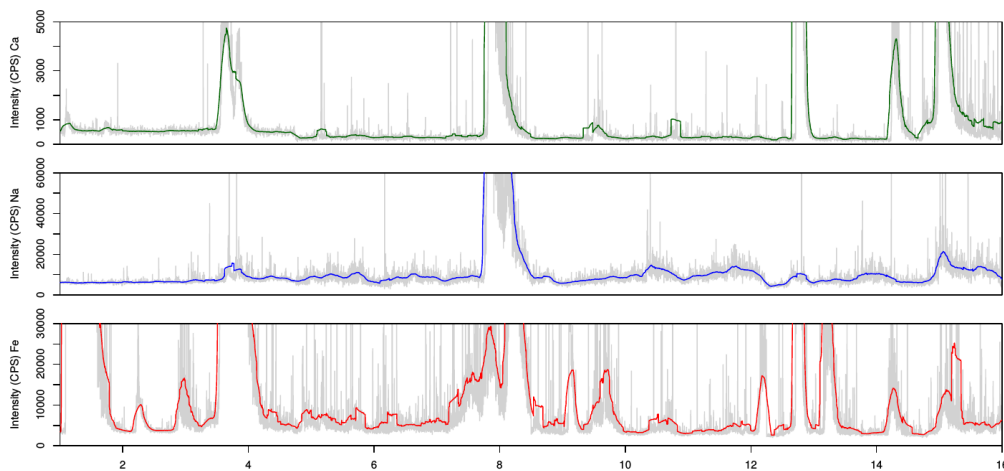


Figure 2: Test measurements of sodium, iron and calcium on ice from Titlis sampling in 2014.

- Data sets for each section should consist of several repeated measurements to be able to draw statistically valid conclusions
- Measurements of several elements:
 - Sodium:** considered representative for more soluble impurities.
 - Iron:** considered a better indicator for more particulate impurities (dust component), very different from calcium in case of Titlis (see fig. 2)
 - Calcium:** considered closely correlated with dust content
 - Sulfur:** earlier measurements (other methods) proclaim higher concentrations within triple junctions (e.g. Mulvaney et al. (1988), for sulphuric acid and using SEM/ED X-ray)

Actual schedule

- June 8: Meeting/Discussion
- June 9: Power outage
- June 10/11: Parameter testing
- June 11/12/17: Measurements on run 48
- June 13/15: Measurements on run 85
- June 15/16/18: Measurements on run 95
- June 18: Measurements on run 100
- June 19: Calibration (unsuccessful, will be repeated)

As an estimate, it took about 4 hours to complete a measurement session (grain boundary and grain interior for 3 elements on 5 grains).

4 Laser parameter testing

A general overview on the setup can be found in Sneed et al. (2015).

The settings for laser ablation ICP-MS on KCC regular down-core measurements are 100 μm laser spot size at 85 $\mu\text{m}/\text{s}$ speed. For the purpose of measurements linked to microstructure we needed to figure out which settings would yield a clear signal while measuring more delicately i.e. along a more precise laser ablation trace.

It is possible to measure “multi-element” or “single element” lines. In the first case the mass spectrometric measurement will yield the counts of several elements from the ablated material of a single trace. This takes much longer than a single element measurement and provides data with much lower resolution. We opted for the single element method, however this means that we had to set more laser paths.

As we want to compare measurements from grain boundaries with grain interiors it is necessary to decrease the spot size for a more locally concentrated signal, this is especially relevant for smaller grains (less than 0.5 mm^2 in diameter). At the same time we need a certain amount of ablated material to get a signal that is well above the noise level and can be interpreted. We tested smaller spot sizes (40, 65, 80 μm) and slower ablation speed (5, 15, 40 $\mu\text{m}/\text{s}$).

A combination of 40 μm spot size at 40 $\mu\text{m}/\text{s}$ worked for sodium and iron; for calcium we used a 100 μm spot size to obtain a relevant signal (as only the stable isotope ^{44}Ca can be measured which comprises about 2% of the natural abundance). For the 40/40 combination we additionally set the focal depth below the ice surface, causing a deeper laser ablation trace and producing more material, while keeping it narrow.

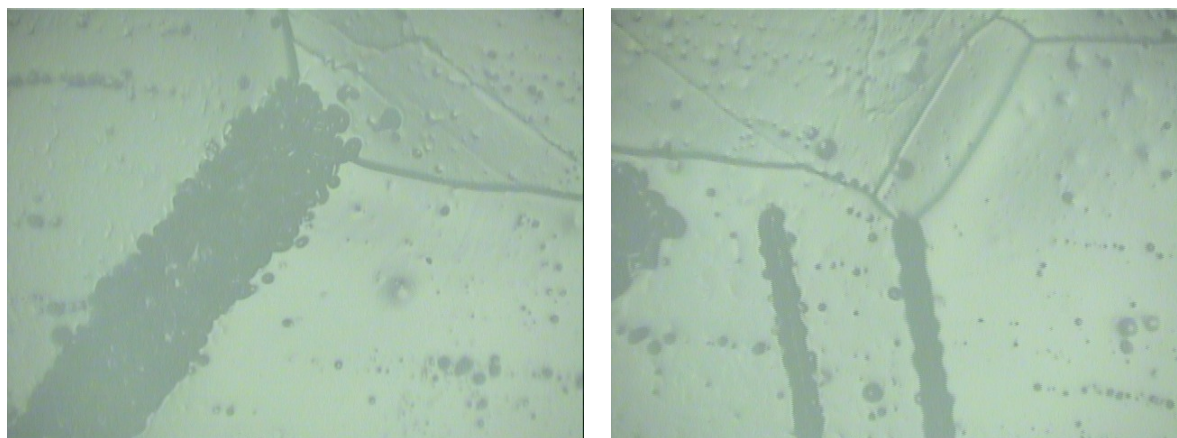


Figure 3: 100 μm (left) and 40 μm (right) spotsizes compared to sublimation groove

5 KCC Samples

As a working hypothesis we assume that the depths derived from the fabric measurements for observed layers can be used to choose the measurement sections, although the surfaces of the two aliquots are perpendicular and some centimeters apart (see fig. 4, thus neglecting the effect of inclined layers on the depth estimates.)

We chose run 48 as a shallower sample from below the firn-ice-transition and run 95 as a deep sample

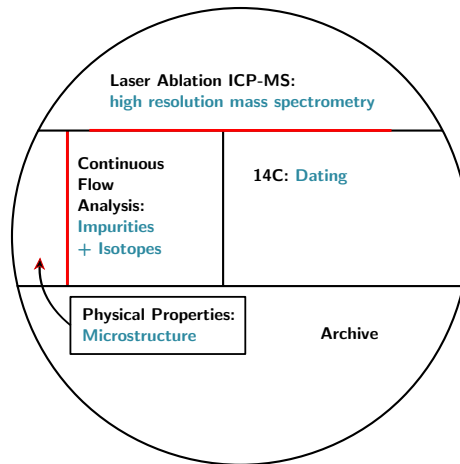


Figure 4: KCC cutting scheme. PP- and LA-aliquot surfaces are perpendicular.

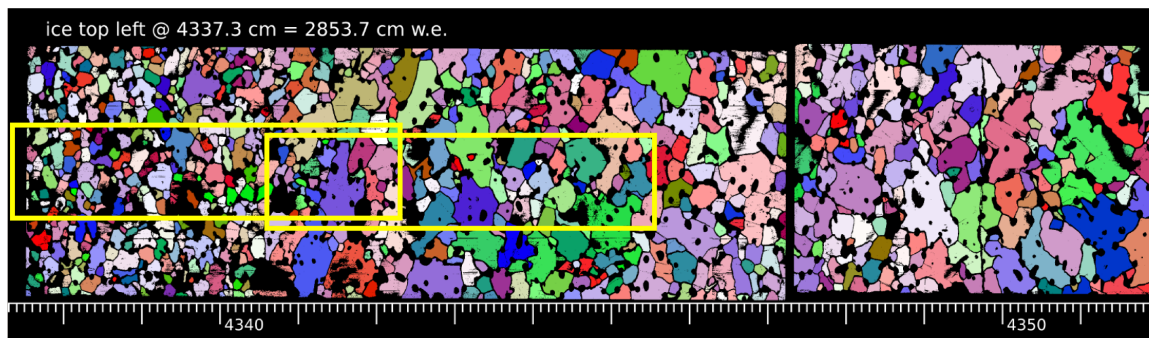


Figure 5: Fabric images of run 48 with depth scale [cm ice]. The size of the sampling area from the laser ablation chamber seal positions is indicated in yellow.

above bed rock; both exhibiting alternating layers of smaller and larger grains i.e. alternating layers of fabric strength.

As two exceptional samples we probed run 85, which shows clear indications for deformation, e.g. layer inclination and elongated bubble shapes, and run 100, showing very small and strongly oriented grains just above bed rock and enriched with dust particles.

See figures 5 to 8 for the fabrics in the depths of the chosen samples and schematic illustration of the seal positions, i.e. measurement fields.

Sample preparation

The chosen pieces of KCC are scraped with a plate from stainless steel to remove frost from storing and irregularities from earlier measurements where the surface sublimated in the ablation chamber.

The sample is taken from the cold lab to the laser lab, placed on the tray and installed in the previously cooled cryocell (-20°C).

By means of a motorised stage the sample is moved and raised to meet the bottom of the ablation chamber. The tightness of the seal, that is created by the contact between the ice and the gasket material, is checked by diverting the flow of carrier gas to a flow meter prior to beginning ablation.

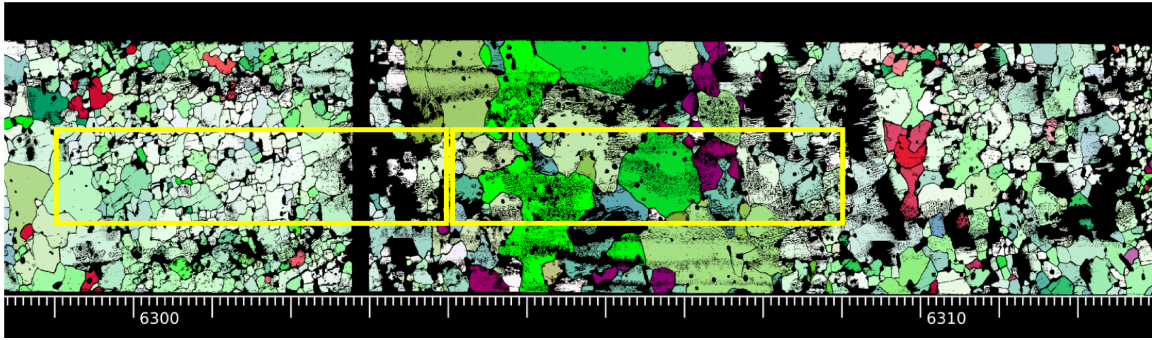


Figure 6: Fabric images of run 85 with depth scale [cm ice].

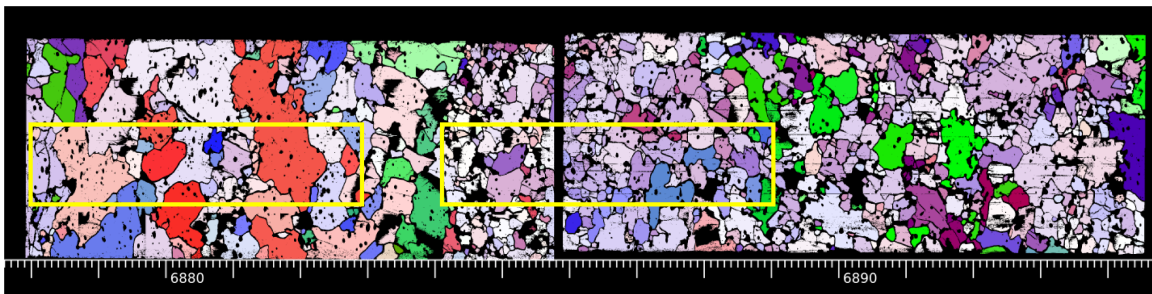


Figure 7: Fabric images of run 95 with depth scale [cm ice].

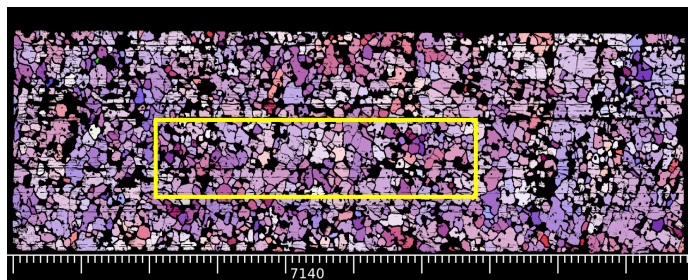


Figure 8: Fabric images of run 100 with depth scale [cm ice].

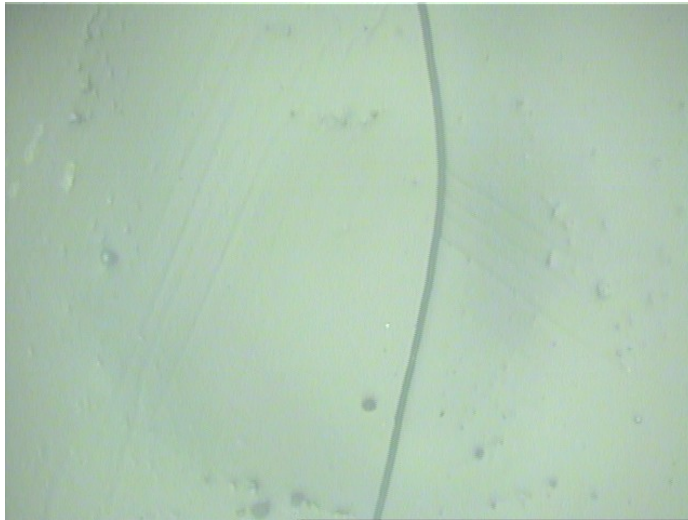


Figure 9: Screenshot from the sampled surface of run 100. Apart from the clear sublimation groove at the grain boundary, several oriented subgrain boundaries are emerging.

Ice surface

The camera of the laser ablation unit shows a constant image section of $640 \times 480 \mu\text{m}$.

Depending on the humidity in the laser lab and likely also on ice properties the surface appears rough at first and no microstructural features can be distinguished. Due to the rather fast sublimation in the ablation chamber the surface smoothens quickly though and after about half an hour grain boundaries (i.e. sublimation grooves) appear as clear dark lines. Subgrain features can also be observed as sublimation continues. An exemplary screenshot (Fig. 9) illustrates how the surface looks at the best observed quality.

As it is not possible to zoom out it is rather difficult to get an overview (by scrolling, i.e. moving the ice relative to the camera, in all directions) of the grain assembly. For some of the measurement sessions videos could be recorded to provide a more complete description of some of the investigated grains if necessary.

The focus of the camera has to be adjusted after lateral moving of the stage to maintain a sharp image and simultaneously to set the laser's focal depth at several points of a line to ensure equal volumes of ablated material all along that line.

Depth assignment

The desired measurement depth which was determined from the fabric images in advance is marked at the aliquot's outer rim in the cold lab as visual guidance (acrylic glass on top of cryocell casing) for the positioning of the seal on the ice surface. This is based on the assumption that even for inclined layers the depth estimates from the fabric images are valid for the laser ablation aliquot.

During a set of measurements (seal at fixed position) the coordinates of the stage relative to the laser are noted for the begin of each single measurement. At the end of a set of measurements a straight long line ($85 \mu\text{m}$ spotsize, perpendicular to core axis) is drawn with the laser which is visible on the ice surface with the naked eye. In the cold lab the offset of this "depth anchor" line in reference to the original depth marker on the sample piece is measured. Subsequently, the depth of all measured features can be

calculated.

6 Measurement pattern

The laser control program offers the option to set straight lines, single spots and cranked paths for the laser measurement which enables us for example to follow grain boundaries. We designed different measurement patterns, explained below, to investigate different hypotheses. An overview is provided in table 1. For details on individual measurements see the measurement logging table (separate file).

Table 1: Overview of measurements. Weak/strong fabric \equiv less/more oriented grains, see fig. 5 - 8 for visual comparison.

Run	Microstructure	approx. depth [m]	Elements	Pattern	Mean grain size [mm ²] \pm standard dev.
48	larger gr., weaker fabric	below 43.40	Na, Fe	gr.	
48	small gr., stronger fabric	above 43.40	Na, Fe, Ca, S	gr.	2.48 \pm 0.76
48			Na, Ca	var. lines, mesh	
85	large gr., weak fabric	below 63.04	Na, Fe, Ca, S	gr.	25.21 \pm 33.71
85	small gr., strong fabric	above 63.04	Na, Fe, Ca, S	gr.	2.15 \pm 1.81
95	large gr., weaker fabric	68.78 - 68.83	Na, Fe, Ca, S	gr.	12.14 \pm 10.10
95	smaller gr., strong fabric	68.84 - 68.89	Na, Fe, Ca	gr.	2.41 \pm 3.63
95			Na, Fe, Ca	var. lines	
100	small gr., strong fabric	71.40	Na, Fe, Ca	grains	0.98 \pm 0.69

6.1 Grains

For each seal position on a layer of certain microstructural characteristics we picked 5 grains.

Although we speak for example of “layers of well-oriented grains” this is to be understood in a statistical manner. By picking 5 grains (without any indication of their individual orientation) within such a layer we can not guarantee that all of them are representative for the overall layer characteristics. We tried to pick grain boundaries of varying orientation, i.e. running perpendicular/parallel/diagonal relative to the ice core axis. We estimated the length of the “half-axes” of each grain to later be able to calculate a grain size estimate. See fig. 11 for an exemplary illustration of the measured traces.

Sodium, Iron and Calcium were generally measured along different boundaries of each grain and either along a path parallel to the previously measured grain boundary (150 - 250 μ m distance) and/or along a spiral raster set roughly in the center of the grain. Ablation times for the set paths were between 20 and 60 seconds and noted exactly.

Sulfur was measured in spots set on triple junctions and in spots set in some distance towards the grain interior for comparison. LA ICP-MS measurements for sulfur had been known to have a high background which prevents accurate measurements of the concentration of small volumes, thus we did not consistently measure sulfur for all sections.

6.2 Variability lines

For the purpose of comparing the signal variability between layers of different microstructural properties we measure long lines of 7 or 8 cm that run parallel to the ice core axis and pass through the depth of a

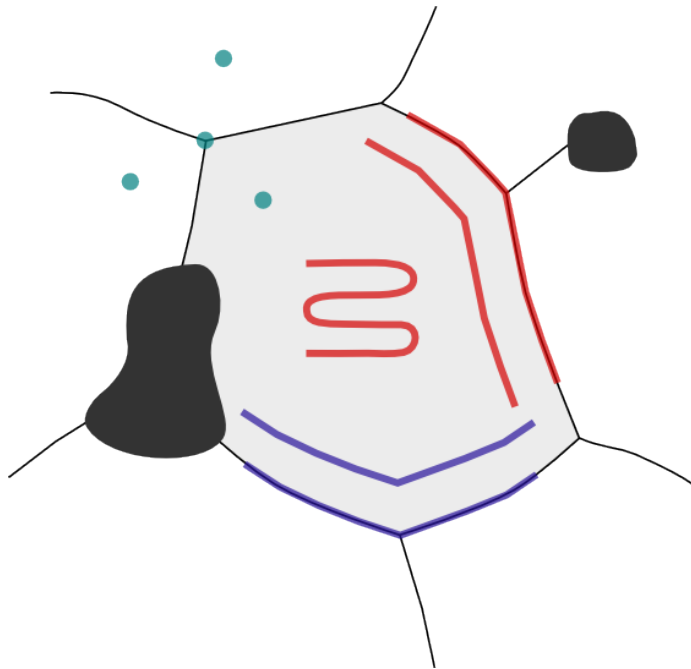


Figure 10: Sketch of measurement coordination at a typical grain setting: Sulfur spots on and opposite of triple junctions (green), lines on and parallel to grain boundaries (blue, red), grain interior raster (red); blue and red would correspond to two different elements e.g. sodium and iron.

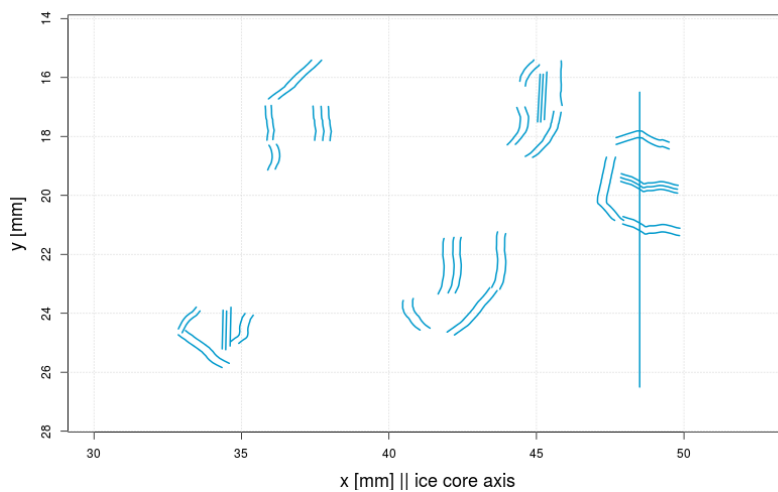


Figure 11: Traces plotted from coordinates collected during the measurement of a large grain section. Traces for three elements and three features (GB, PL, ML) for five grains can be distinguished. The vertical line is used as “depth anchor”.

clear layer transition (i.e. with strong contrast in grain size) as determined from the fabric images. Shorter lines of about 1 cm that cross several grain boundaries were measured and the cross points noted.

6.3 Mesh

To test if lateral changes can be visualised as a two-dimensional map we set up a mesh of several horizontal and vertical lines covering an area of a few cm².

7 Calibration

To be completed.

8 Methodological comments

For specific information on the technicalities of laser equipment, mass spectrometer etc. refer to Sneed et al. (2015).

Washout time The ablated material takes typically about 12 seconds to reach the mass spectrometer – that is called the washout time. It is not straightforward at this time to connect individual spikes in the ICP output to very small features on the camera.

To bypass having to deal with this issue we decided to measure within a microstructural feature, e.g. along a grain boundary, instead of crossing different features, e.g. measuring along grain radii. This also enables us to collect much more material for each feature, which can be interpreted as a statistically evaluable sampling.

Laser path setting The laser control program offers the option to set cranked paths for the laser measurement which enables us to follow grain boundaries. However, the path sometimes deviates from its original position relative to the ice surface when moving the stage in order to extend the path. This is probably due to imprecision of the stage motors on the μm -scale. In order to have the path outline in the desired shape and at the exact position a time-consuming fine-tuning of the stage for each path is necessary (for a fine spot size).

Measurement recording It is possible to record the whole measurement session on video and the coordinates of all set laser paths (for a fixed seal position) can be saved to file which eliminates the need to log the coordinates manually and facilitates the subsequent depth calculation.

Surface preparation A possible advancement for future measurements of this kind would be the use of a customized microtome to smoothen the ice surface for a better image and to ensure that the amount of material ablated at each point is the same.

Sample choice The choice of sections to be measured is firstly guided by the microstructural structure to be investigated but, if possible, earlier measurements (CFA, axis-parallel laser ablation) should be also considered in order to not pick depths where impurity concentrations are already low compared to the mean level.

Sample transport Ideally, the cryocell would be inside the cold room or directly connected to it to be able to transfer the sample directly without leaving the cold room environment. This could prevent frost and melt on the surface.

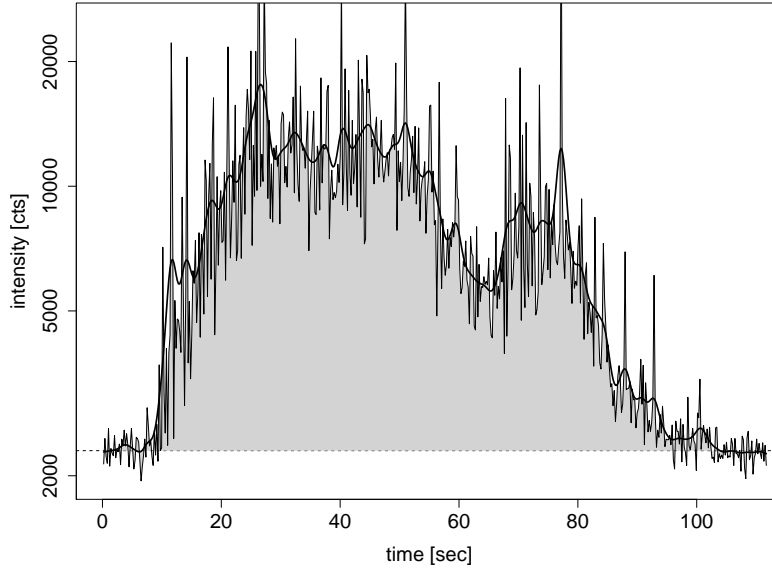


Figure 12: Raw data is very spiky and smoothed data is used for illustration (see appendix). A gaussian kernel with bandwidth of 2 seconds (i.e. ~ 10 data points) is used for smoothing. The shaded area is integrated.

9 Preliminary findings

We show the first results from the measurements. The data is recorded as counts per time. The recording times were (mostly) chosen well above the ablation time for set paths to be sure to have collected all data with the mass spectrometer. The signal should always begin and end on a noise level that is characteristic for the element to be measured and might depend on other technicalities.

9.1 Grain concentration gradients

We want to estimate the local impurity content by assessing the integrated signal for each feature, normalized to the duration of ablation.

We first correct the raw data of each data set by subtracting the background that is estimated based on the mean of the last 50 data points, i.e. the last 10 seconds, or the first 6 seconds, depending on which value is smaller.

The integral is calculated from the raw data where background is subtracted. For each measurement the individual duration and speed of ablation was noted and is used to calculate the “impurity content per length ablation path”, henceforth referred to as “content” (in counts per millimeter) in order to be able to compare the data quantitatively.

Fig. 12 and 13 illustrate the data processing and visualization.

Individual display of all data for each grain can be found in the appendix (fig. 32 to 38) and 40 to 47. For the following comparison data was separated according to the spot size of the laser, i.e. 40 or 100 μm . Considering a semi-spherical shaped ablation trough, the amount of ablated material should be larger by a factor of $2.5^3 = 15$ for the larger spot size. Based on the few measurements we can confirm a factor

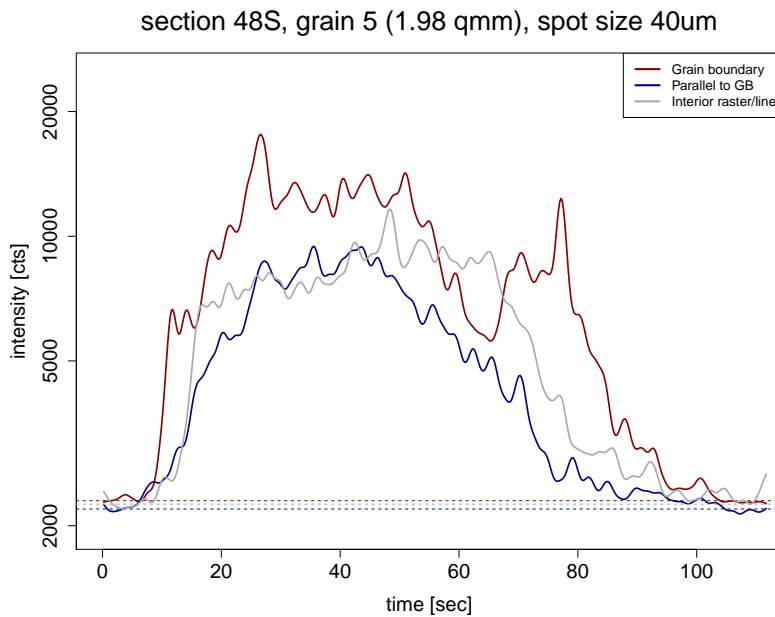


Figure 13: Exemplary data of three features in one grain. The calculated background level for each measurement is indicated; the values vary slightly in this example. The grain boundaries are clearly enriched in sodium, while the grain interior is depleted; this pattern holds true for the majority of the collected data.

of the order of 10, but varying strongly.

Fig. 14 and 15 show the background for sodium for the two applied spot sizes. Generally the background level is below 3000 cts with the exception of the measurement for section 48L. When comparing with fig. 16 the question arises if the signal level is independent of the background level.

Fig. 23 to 25 (appendix A) show the changes of sodium content with depth for the different features, also indicating the size of the data set (number of grains) used for the calculation. Fig. 16 and 20 summarize the information of fig. 23 to 25.

Fig. 18 and 21 illustrate the ratio of impurity content in grain boundaries to the impurity content parallel to grain boundaries. See fig. 31 and 39 for indication of grain numbers.

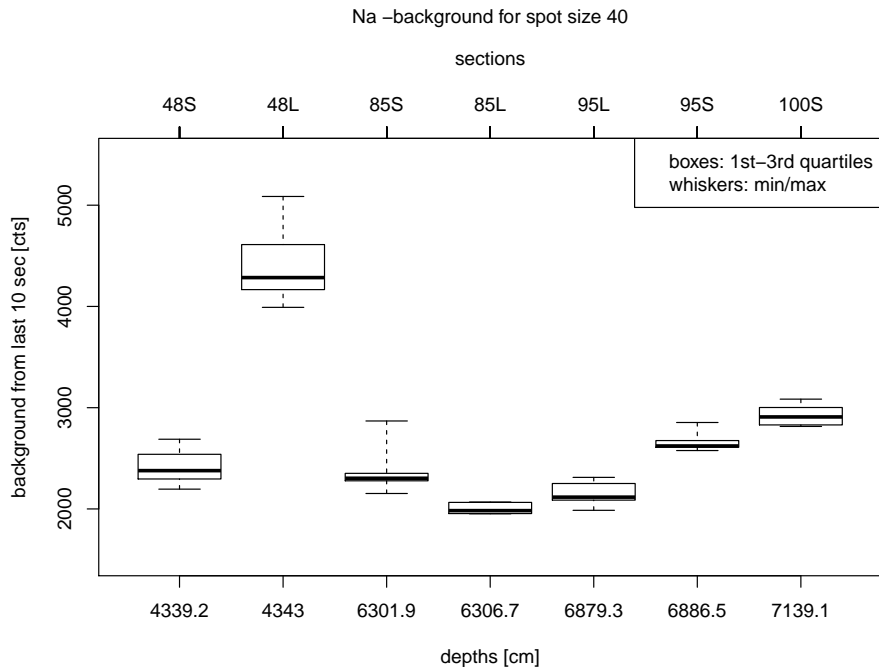


Figure 14: Background level range for each section/depth as calculated from last 10 seconds (or first 6 seconds) of each measurement in the section where a spot size of 40 μm was used. Boxes are bounded by first and third quartiles, while median values are indicated and whiskers extend to minimum and maximum values.

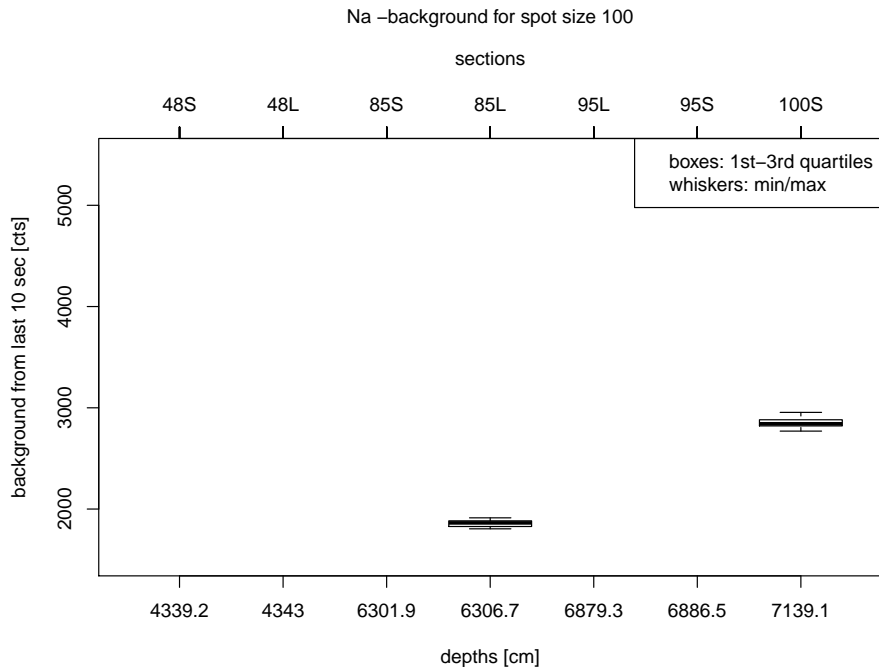


Figure 15: 100 μm was applied only in two sections. The values do not seem to differ significantly from the background when using a smaller spot size (fig. 14).

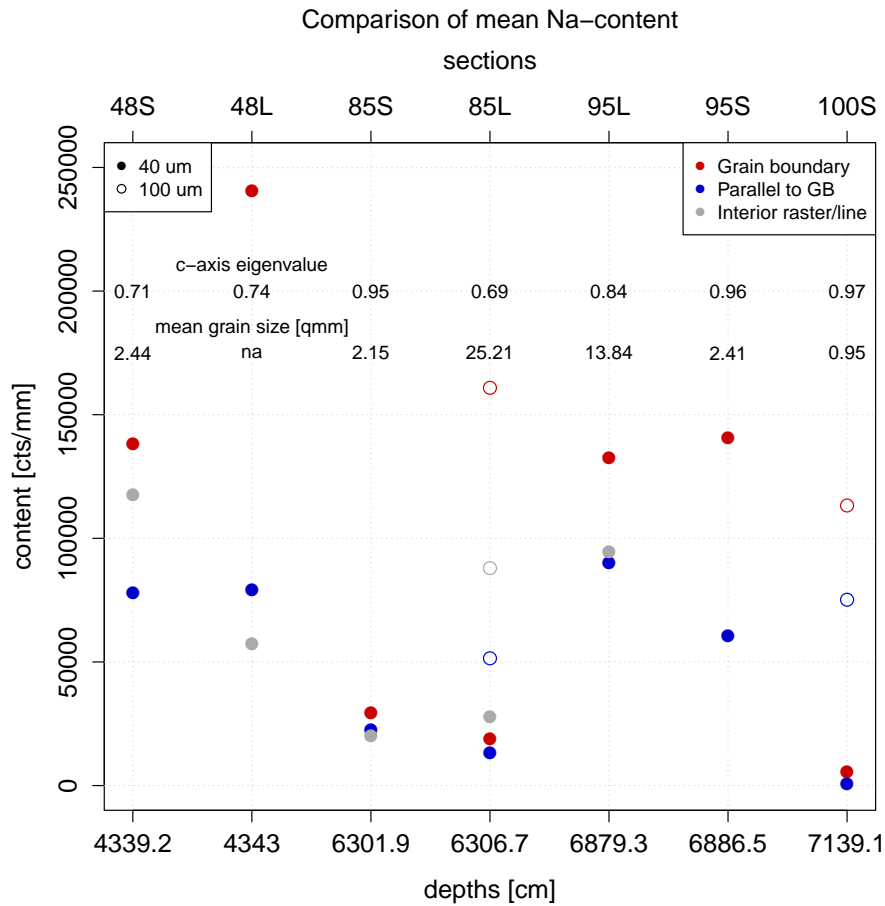


Figure 16: Summary of the mean integrated and normalized sodium content of all features in all sections. The spread of the single values for each feature and section is shown in fig. 23 to 25 and should be kept in mind: due to the small sample size outliers significantly alter the mean values. Highest impurity content in grain boundaries and difference to grain interior impurity content is measured for the shallow large grain section (48L). While deep section (95) and shallow small grain section yield similar impurity distribution, the intermediate section (85) has much lower overall impurity content, as well as the bed rock section (100), but for the latter discrete ICP-MS measurements show higher values. The contents for 100 um spot size are much higher, as would be expected (discussed in the text), and can not be compared quantitatively with the other sections but they exhibit the same gradient from grain boundaries towards the interior. C-axis eigenvalues that were calculated from fabric images of the PP aliquot for the 2cm depth interval of the sections are noted in the graph, as well as the mean grain size; while the two microstructure parameter anticorrelate, no causal relationship between spatial impurity distribution and the two parameters can be deduced based on this data.

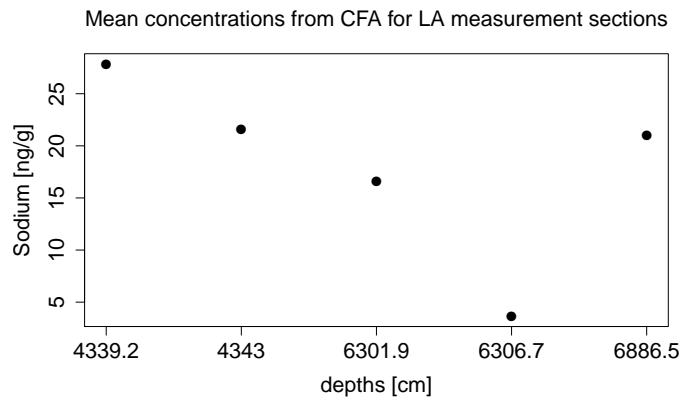


Figure 17: Mean concentrations of sodium as measured with CFA, calculated for the depth intervals of laser ablation measurements. Note that for two depths no corresponding CFA data is available.

9.1.1 Summary and conclusions

Sodium

- Background level seems to be independent of spot size used for ablation which confirms the expectation as background should be a function of how much an element contributes to the sublimation in the ablation chamber.
- Sodium content is – on average – always higher in grain boundaries than parallel to grain boundaries, i.e. 150-250 μm towards the grain interior.
- Between the grain interior (i.e. further than 250 μm from the grain boundary) and parallel to grain boundaries does not appear to be a systematical difference, sometimes the interior is more enriched than closer to the boundary.
- The relative level of sodium content between the sections is comparable to the CFA mean values for the laser ablation measurement sections (see fig. 17).
- The range of calculated values for each feature and section is often rather large (covering several orders of magnitude), implying a spatially heterogeneous distribution of the overall impurity content within the section, i.e. from grain to grain. The sections are between 1.9 and 3.6 cm thick which is enough to hold several annual layers as estimated from layer counting, thus possibly explaining the differences. On the other hand these results could indicate that the lateral variation in impurity content is not negligible compared to annual variation which would have to be considered when interpreting down-core laser ablation signals; this could be an explanation for the observed differences between laser ablation and CFA signal. Further comparison with down-core laser ablation signals are necessary. However, a lateral variation could also be an effect of measurement (dependence of signal strength from the offset of the flow outlet) which needs to be further investigated.
- The sodium content gradient can be observed regardless of the measurement section being a small or a large grain section, i.e. the data apparently does not provide any clues as to understand the development of cm-scale fabric layers.

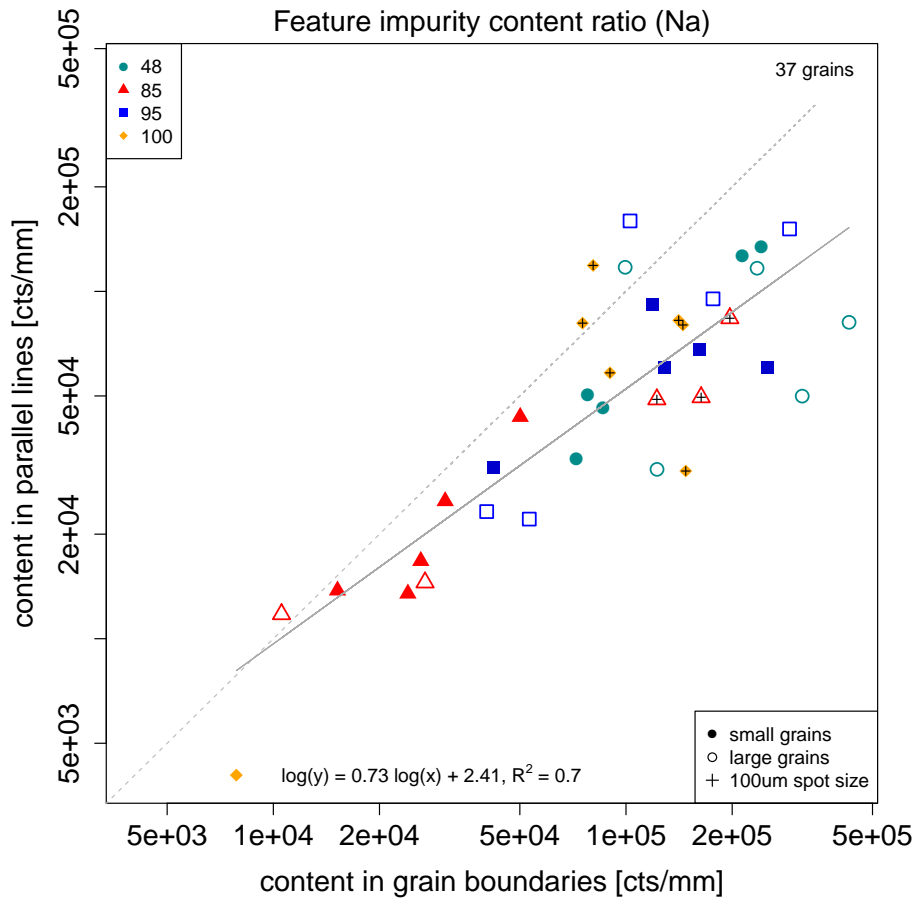


Figure 18: The impurity content (sodium) in grain boundaries is scattered against the content in the associated parallel lines, illustrating their ratio. Each symbolic item represents a GB/PL pair. Filled symbols represent small and open symbols large grains, different symbols indicate the four depths, the larger spot size is indicated by black crosses, both axes are logarithmic, colors are for visual support. There is a linear relationship between the logarithmic sodium content (least square fit as solid gray line, fit parameters and coefficient of determination are indicated; dashed line indicates 1:1 ratio) with the symbols for some sections loosely grouped, but no clear pattern due to grain size.

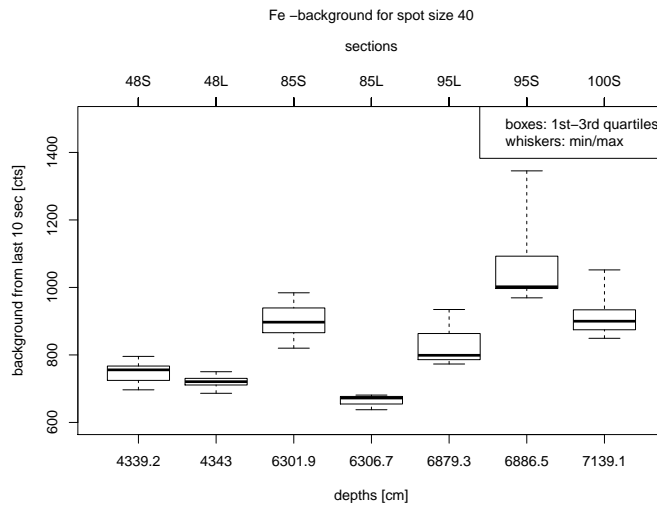


Figure 19: Background level range for each section/depth as calculated from last 10 seconds (or first 6 seconds) of each measurement in the section where a spot size of 40 μm was used. Boxes are bounded by first and third quartiles, while median values are indicated and whiskers extend to minimum and maximum values. Iron background is always lower than the sodium background.

- The bed rock section has lowest sodium values, but discrete ICP-MS (no CFA data available for this section) shows higher values. We hypothesize that this might be an effect of sodium in particles vs. dissolved sodium. The discrete samples were acidified and left for some time, which could be enough to disintegrate sodium-rich particles from bed rock.
- The ratio of logarithmic sodium content in parallel lines to the logarithmic sodium content in grain boundaries can be approximated with a linear fit. We hypothesize that for a given total sodium content in a grain the fractionation in grain boundary and grain interior follows some yet undefined law. Following the assumption that sodium is mainly present as soluble impurity this law could be chemically driven.
- It can not be excluded that the observed spatial gradient in grains is the result of surface diffusion during ice storage. This would probably also eliminate any other distribution that developed in situ. However, the fact that we observe outliers in most sections would argue against that.

Iron

- The bed rock section is enriched in iron. We conclude that particles from bed rock contribute to the iron signal here and regard the corresponding values as outliers.
- Background is always lower than the sodium background which indicates that iron will less readily leave the surface during sublimation in the ablation chamber.
- Iron content does not differ as much between grain boundaries and parallel lines – the least squares fit returns a 1:1 ratio for the sections above the bed rock section. Some outliers (e.g. 95S-grain4, 48S-grain7) could have a strong effect on the mean values which need to be treated with caution (cf. fig. 40 to ??). As apparent from the smoothed data for each grain, often the signal is dominated by narrow peaks which we interpret as originating from particles.

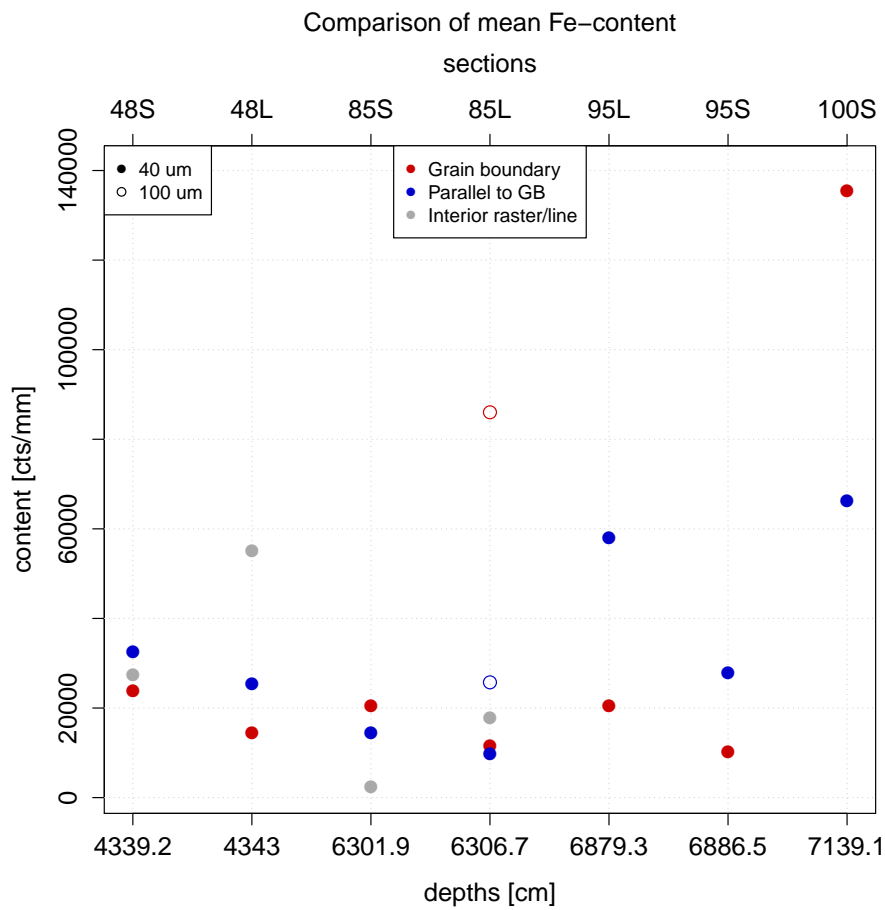


Figure 20: Summary of the integrated and normalized iron content of all features in all sections. Highest iron content is measured for the bed rock section (100S), lowest for the intermediate section (85); both show higher content in grain boundaries. However, for shallow (48) and deep (95) section iron content is lower in the grain boundaries than towards the interior, regardless of grain size. Caution: the presented mean values are highly influenced by peaks and individual grain data should be considered (see fig. 40 to 47)!

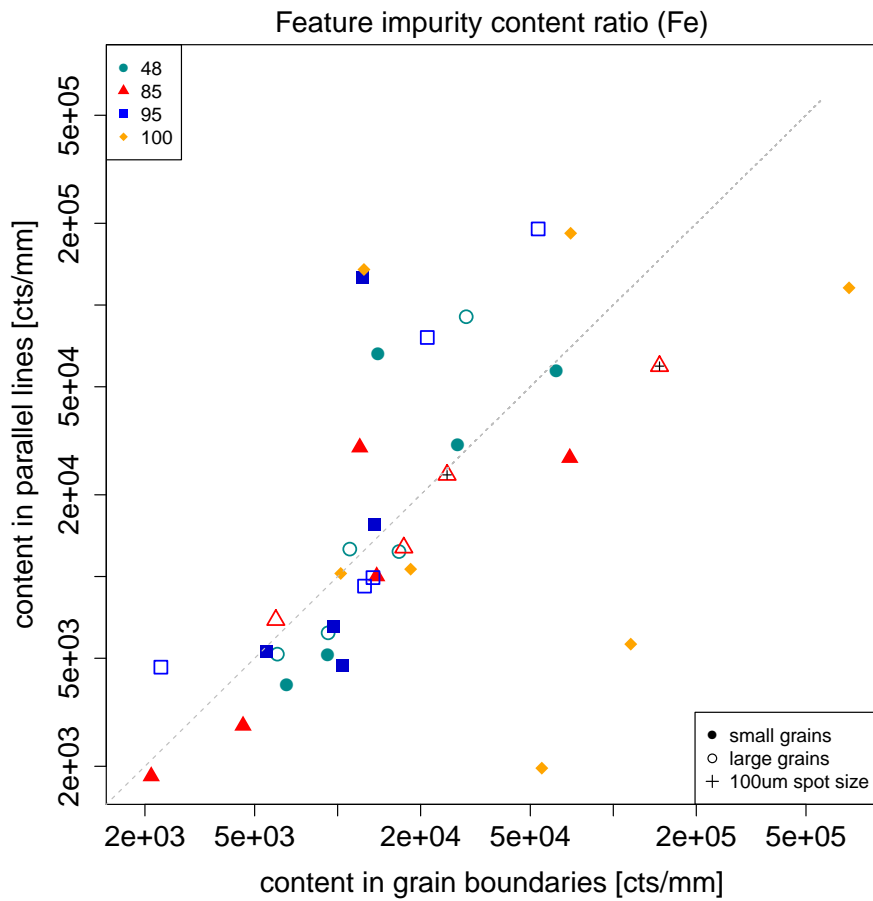


Figure 21: The impurity content (iron) in grain boundaries is scattered against the content in the associated parallel lines, illustrating their ratio. Each symbolic item represents a GB/PL pair. Filled symbols represent small and open symbols large grains, different symbols indicate the four depths, the larger spot size is indicated by black crosses, both axes are logarithmic, colors are for visual support. Several grains from the bed rock section appear as outliers with much higher grain boundary iron content.

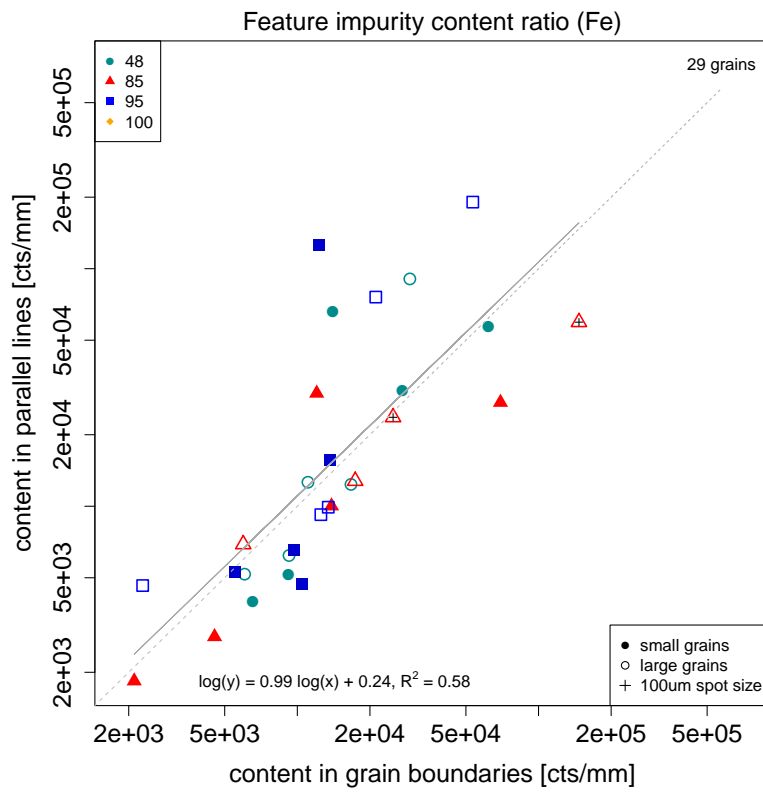


Figure 22: Data presented as in fig. 21, excluding the bed rock section. Linear fit for all depths, excluding the bed rock section, yields an almost 1:1 iron content ratio for grain boundaries and parallel lines.

- A pattern as observed for the sodium does not appear, thus leading to the conclusion that iron is indeed more particulate and less chemically interactive.
- The data per grain show many different patterns compared to the sodium data and is more difficult to classify. In some cases the grain interior is enriched compared to the parallel lines and grain boundaries.
- From a microstructural point of view the many different distributions could be an argument for particulate impurities being more subjected to microstructural processes like recrystallization. This “mechanical/recrystallization mixing” would be dependent on grain boundary mobility which is a function of temperature, stored strain energy and particle size. Above a temperature of about -15°C grain boundaries have been seen/described to be more “sticky”, assumed to be of possibly thicker, quasi-liquid structure (pers. communication Ilka Weikusat and Sergio Faria). Modeling on the micro-scale has shown the heterogeneous distribution of strain energy in the ice matrix. From LASM images it becomes clear that within a section neighboring grains can show quite different levels of subgrain activity, indicating this heterogeneous strain distribution. Laser ablation experiments should be done on a microtomed section where a LASM (or comparable) image was recorded beforehand to be able to investigate this hypothesis by taking into account the amount of subgrain structures.
- On the other hand it could also indicate that particulate impurities are distributed regardless of microstructural features, thus explaining the seemingly random results for the grains within one section.

9.1.2 Open questions

- Why do we see sometimes similarities between data from different features of one grain? Is this a surface roughness (ridges) effect? Or an indication for impurity distribution along the basal planes in grains? Or is it depending on the grain boundary orientation with respect to the assumed conserved impurity layering?

9.2 Laser ICP-MS signal variability

To be completed.

9.3 Impurity mapping from mesh data

To be completed.

A Comparison between sections for each feature

A.1 Sodium

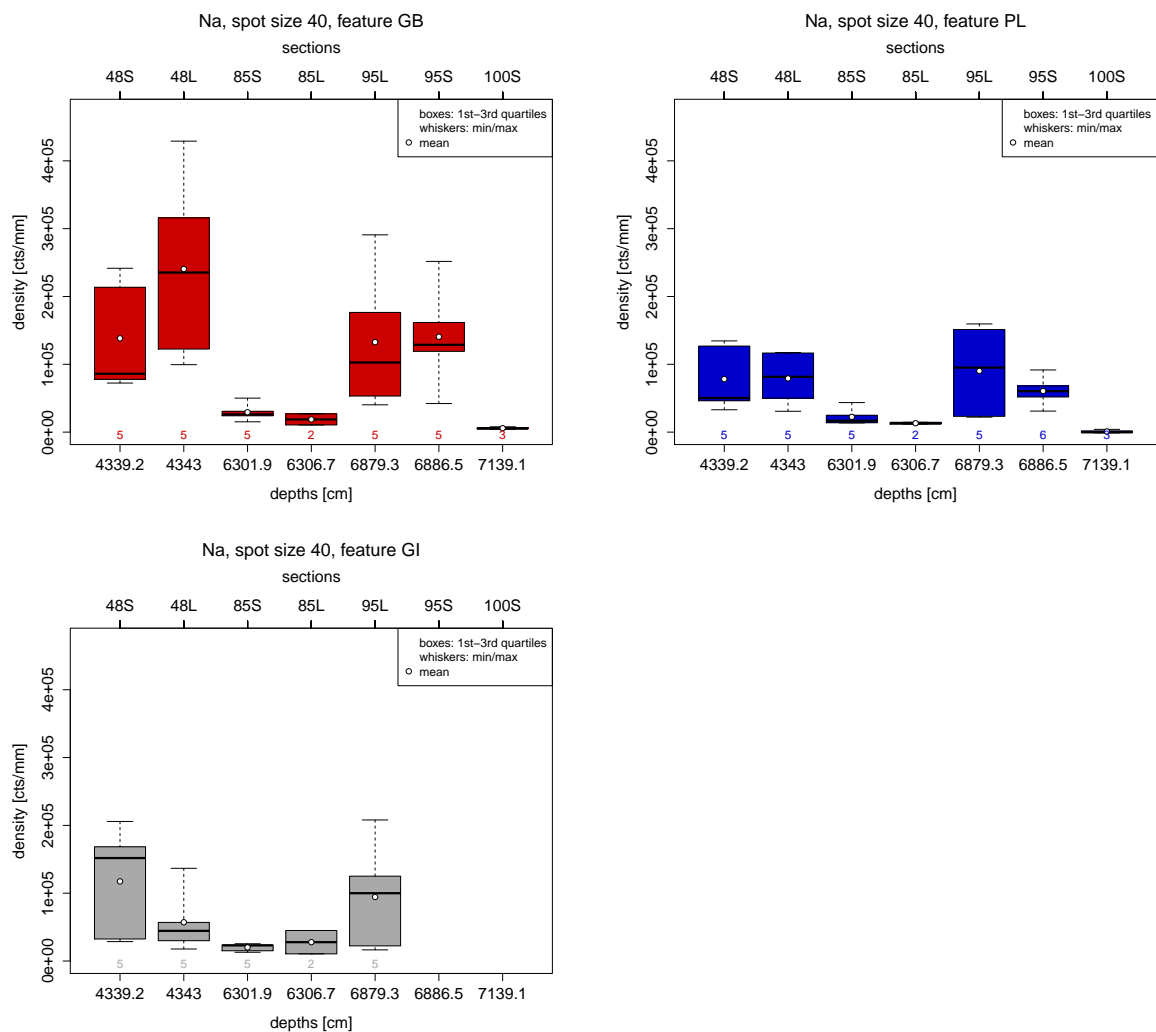


Figure 23: For each depth/section (where “S” or “L” indicates a small or large grain section) the range of sodium content for the respective data set is shown as box-and-whisker-plot, the mean value is given as white dot. The number of grains contributing to the presented distributions are given in colored numbers. Middle lines (ML) and interior rasters (R) were not measured for the deepest sections.

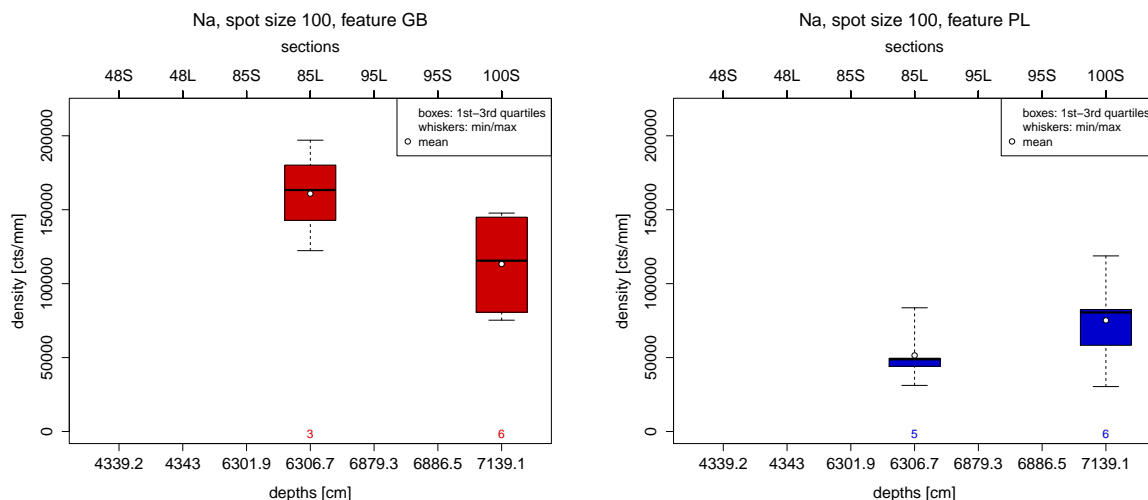


Figure 24: Cf. fig. 23.

A.2 Iron

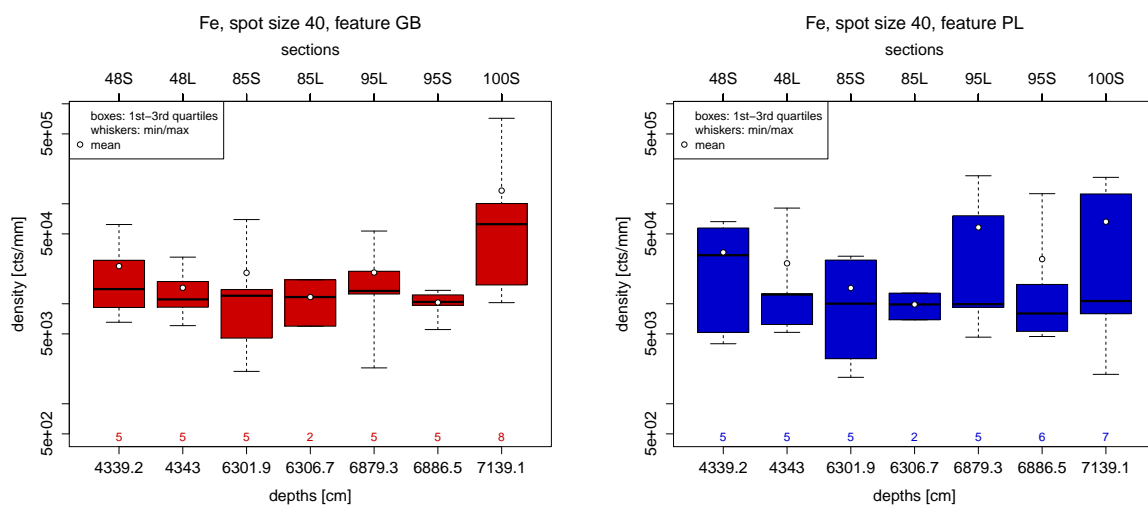


Figure 25: For each depth/section (where "S" or "L" indicates a small or large grain section) the range of iron content for the respective data set is shown as box-and-whisker-plot, the mean value is given as white dot. The number of grains contributing to the presented distributions are given in colored numbers. Middle lines (ML) and interior rasters (R) were not measured for the deepest sections.

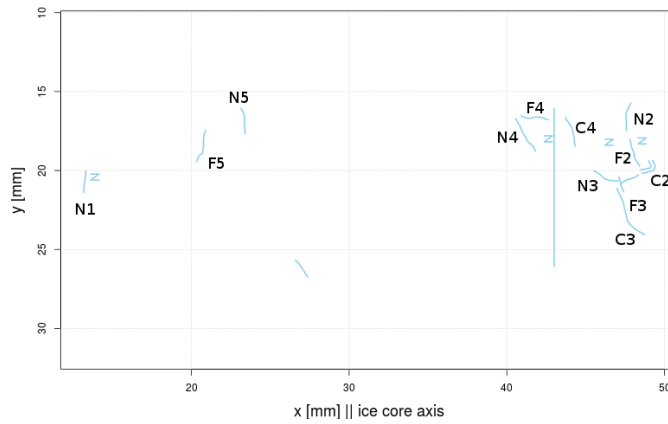


Figure 26: Section 85L: only part of the measured traces was saved for this section. N/F/C indicate the parts of grain boundaries where sodium, iron and calcium were measured; the numbers refer to the grain numbers.

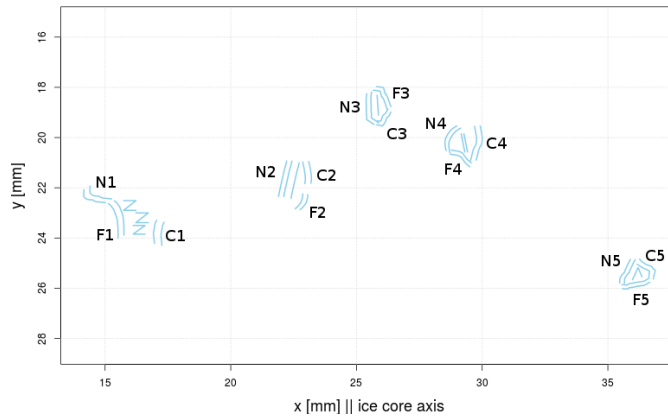


Figure 27: Section 85S.

B Laser ablation traces

Traces that were plotted from saved coordinates from the measurements for part of the measurement sections (not for sections 48S and 48L). Many grains have a roughly hexagonal shape.

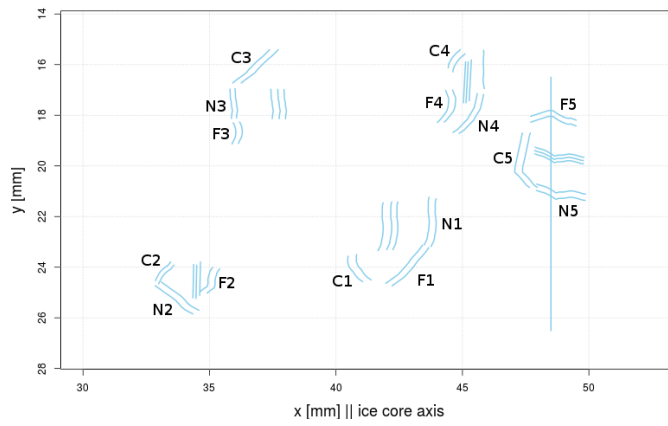


Figure 28: Section 95L.

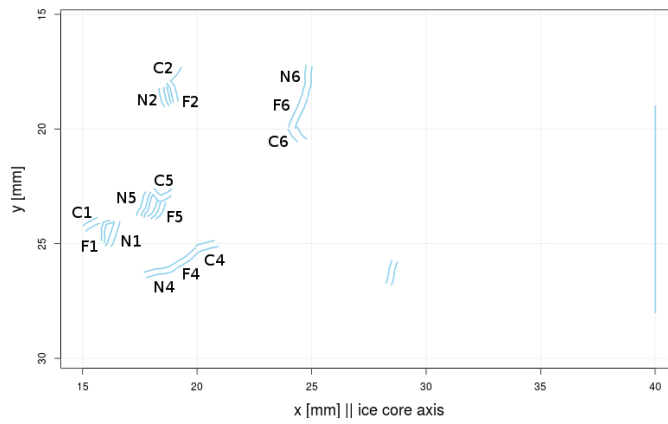


Figure 29: Section 95S.

C Smoothed data for each grain

C.1 Sodium

Data is shown on a logarithmic scale fixed to maximum 25000 counts for better comparison.

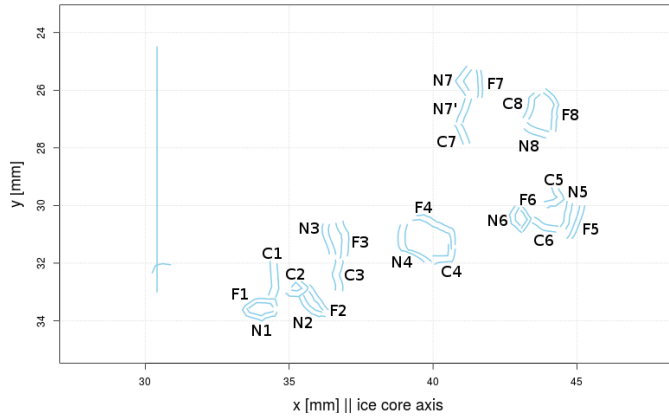


Figure 30: Section 100S.

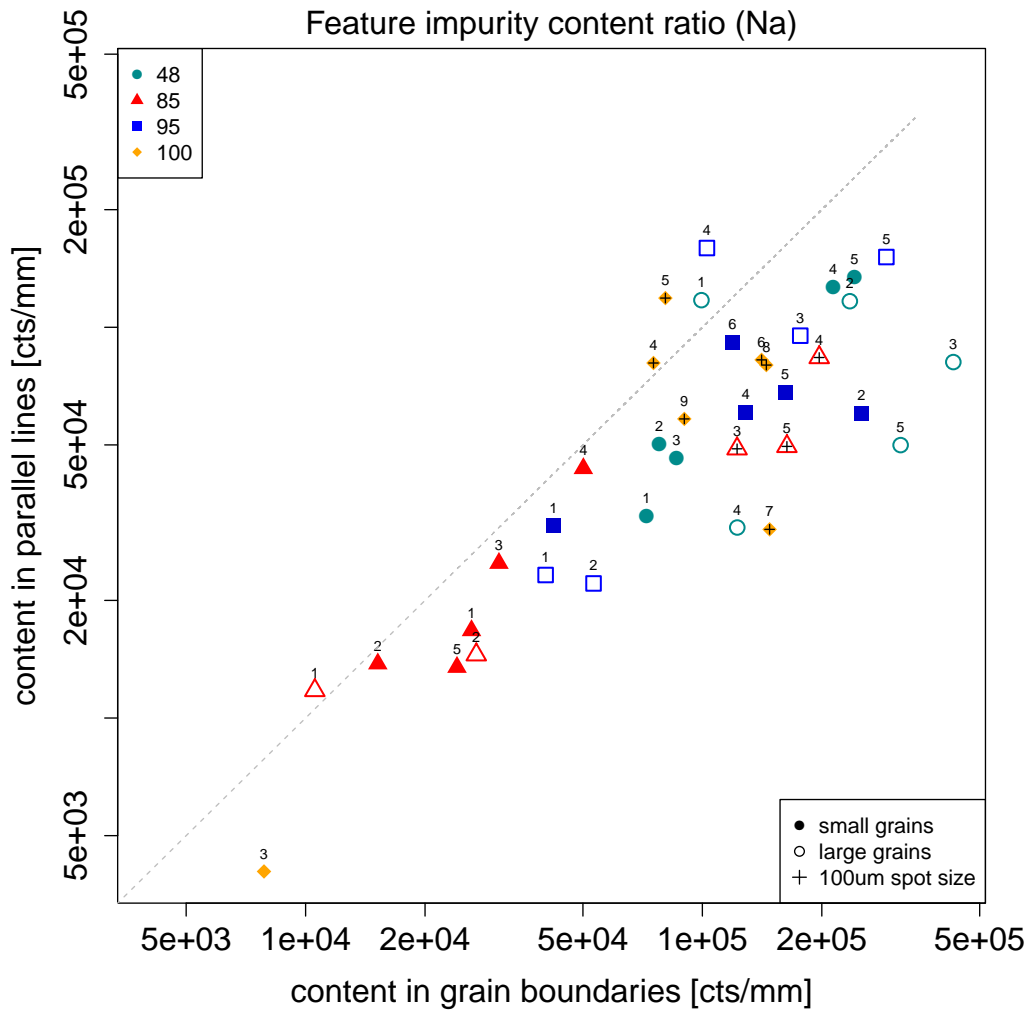


Figure 31: Same fig. as fig. 18 with grain numbers indicated.

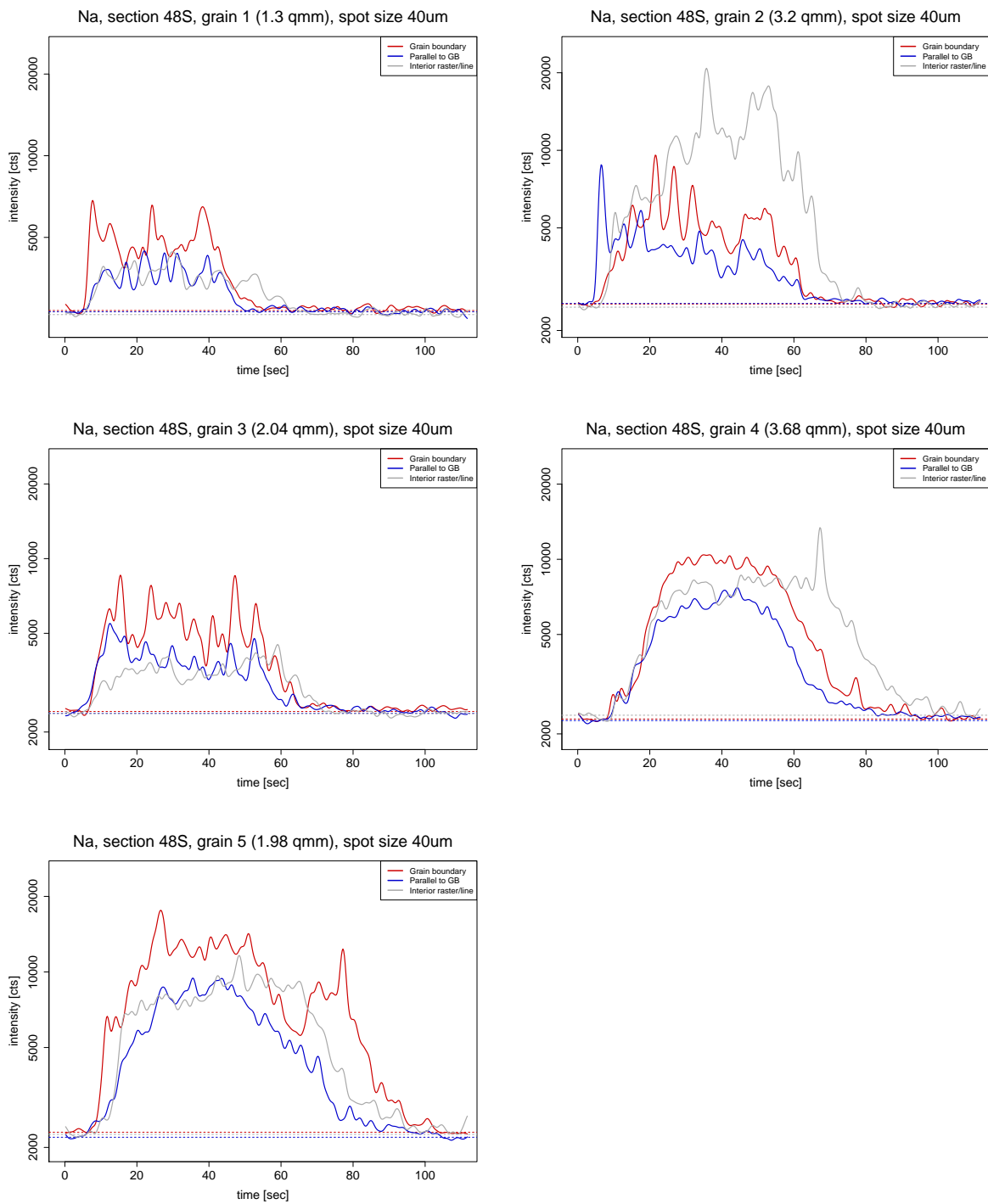


Figure 32: Grain boundaries show mostly higher sodium content than grain interiors. Grain 2 is an exception/outlier to that observation, grain 4 is not clear either – both grains are larger than the others.

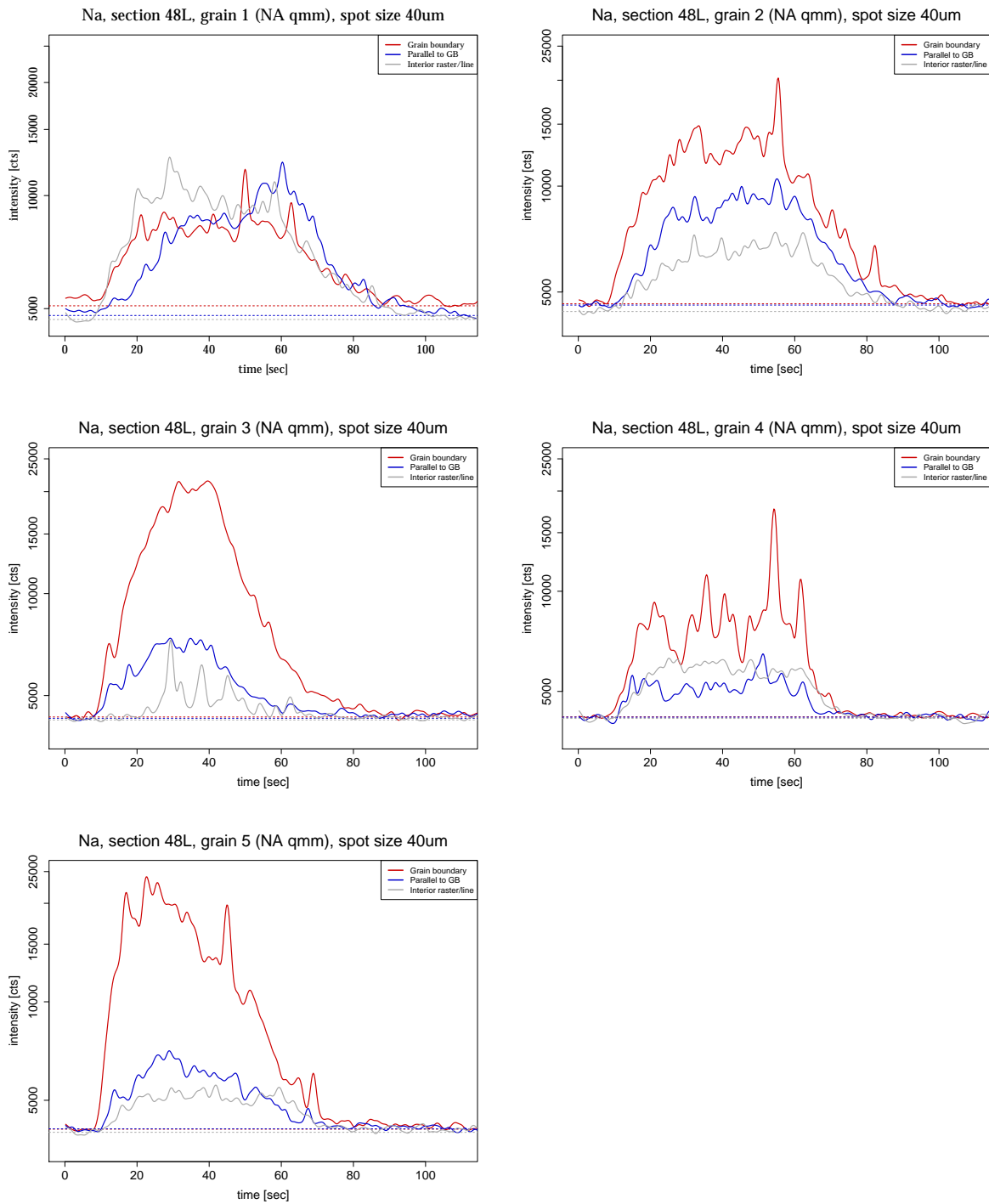


Figure 33: An even larger difference between grain boundary and grain interior can be observed in grains in this large grain section, other than grain 1. For this section no grain size estimates are available.

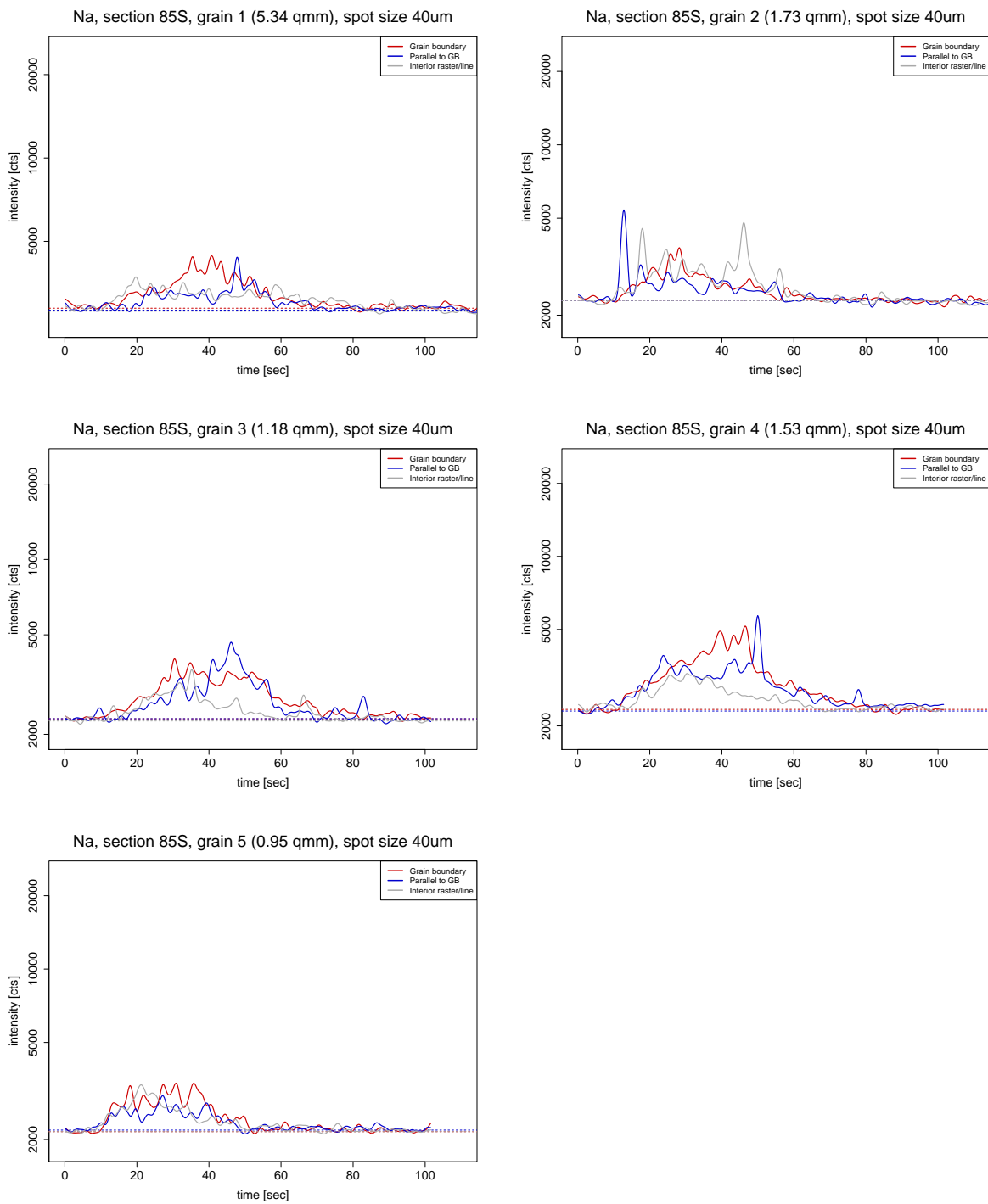


Figure 34: Impurity concentrations are very low in this section. Differences between the features are not immediately discernible.

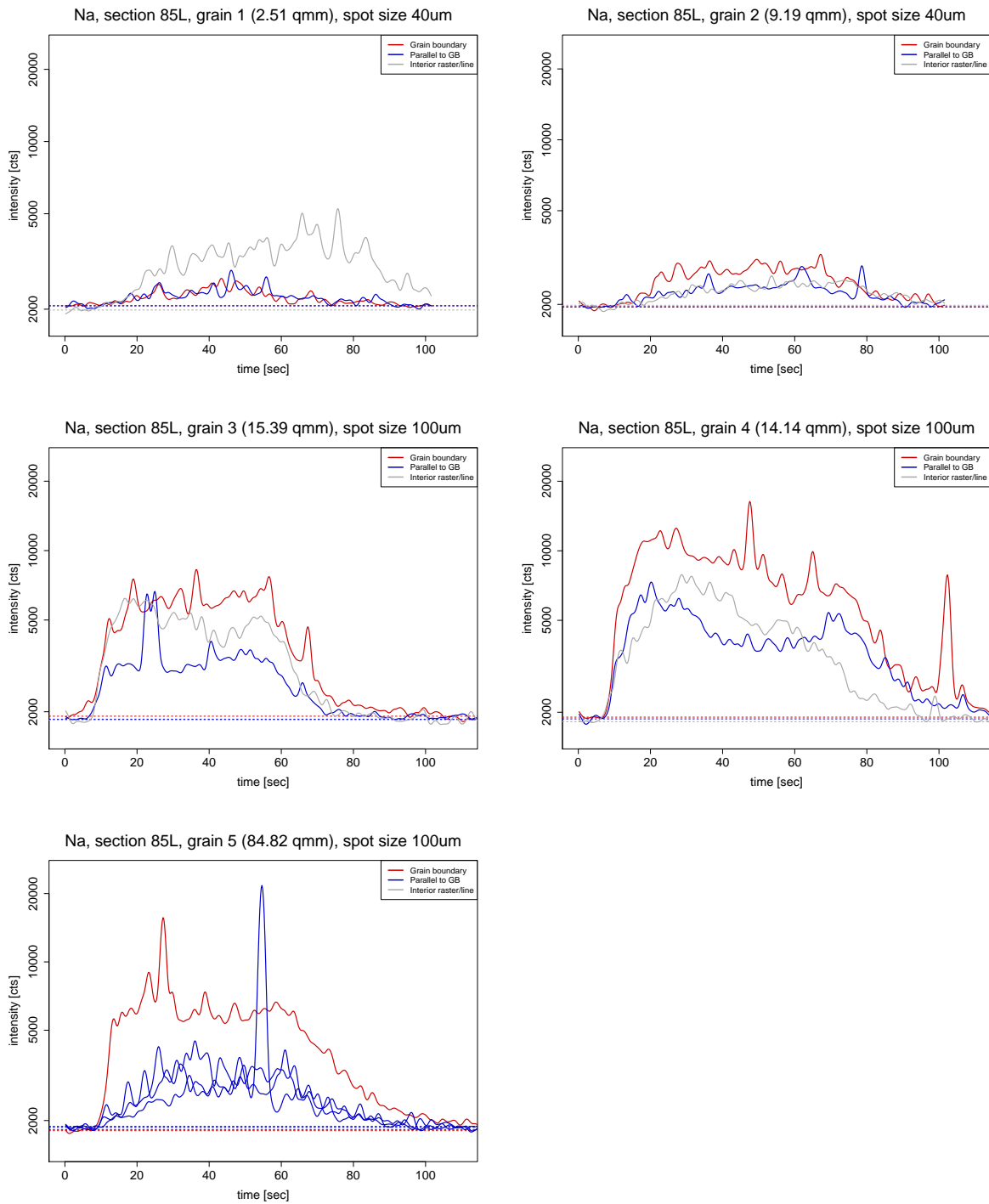


Figure 35: A clear difference in impurity content can be seen in four out of five grains. Grain 5 was an exceptionally large grain and several parallel lines with increasing distance to the boundary were measured. For grain 1 which is the smallest of the data set, the grain interior signal is significantly larger. Grain 3 and 4 show similar signals and have similar sizes.

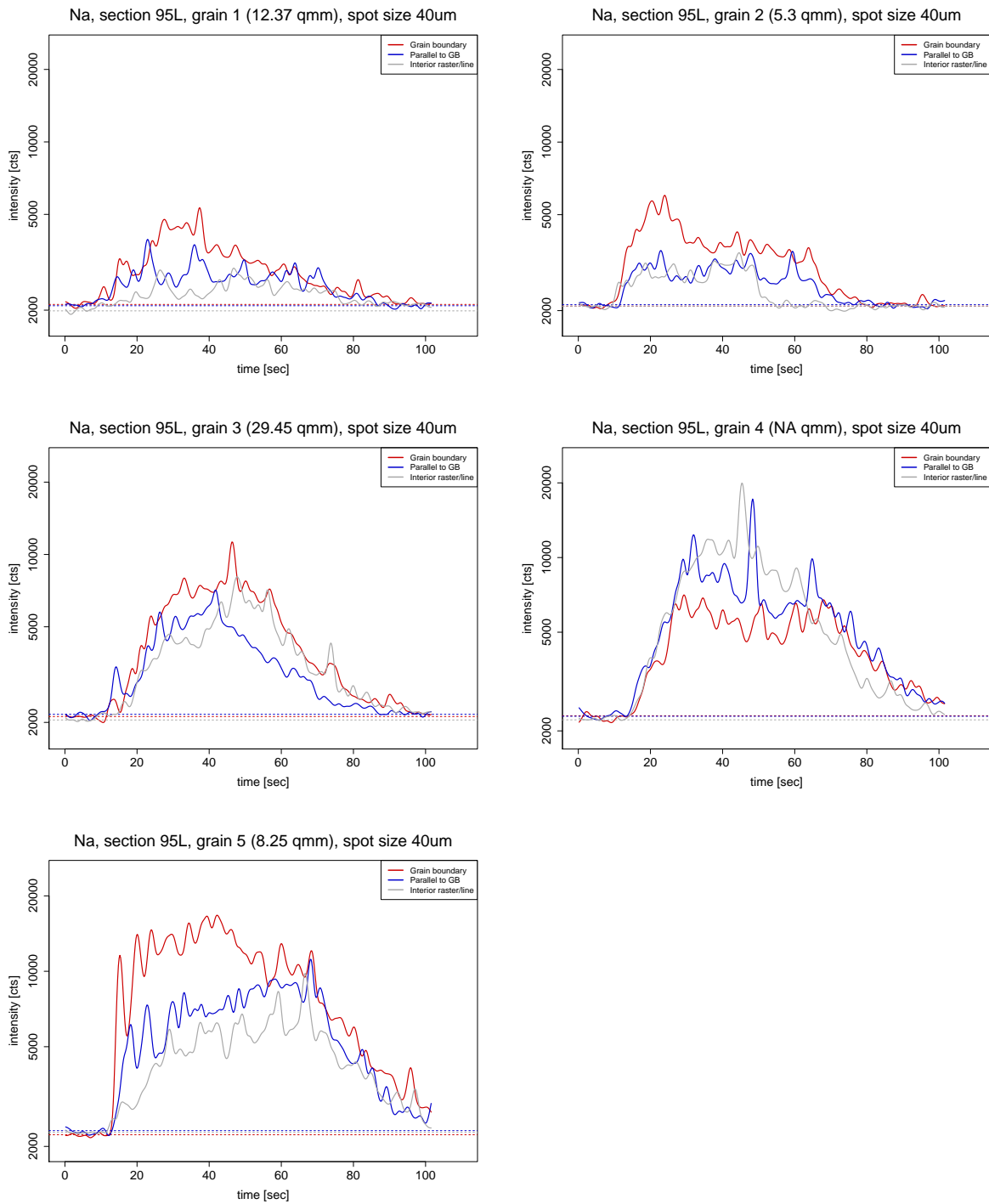


Figure 36: With exception of grain 4 the gradient in impurity concentration can be detected.

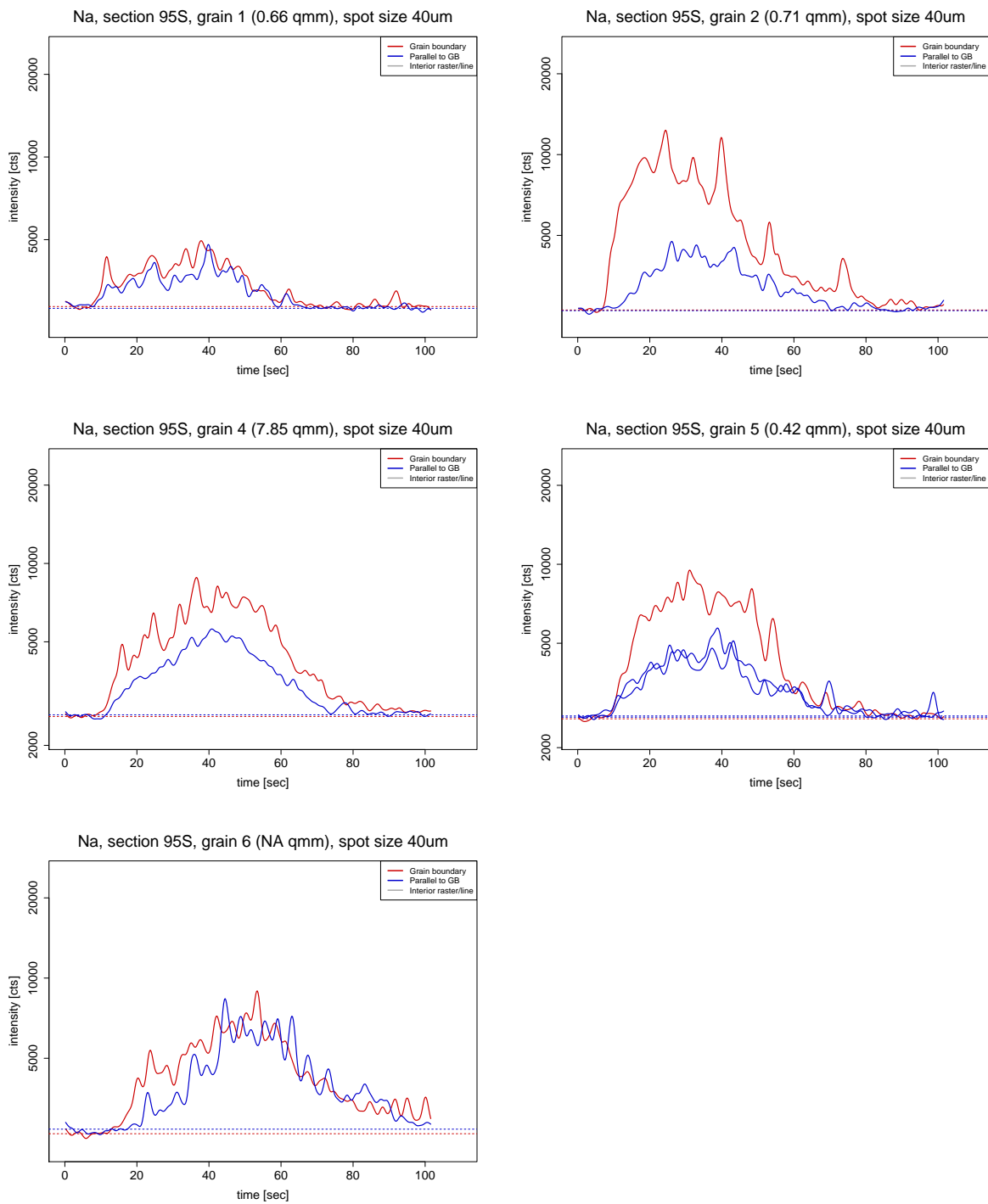


Figure 37: Only grain boundaries and parallel lines were measured for this section. Three out of five small grains show a clear difference between grain boundary and parallel line.

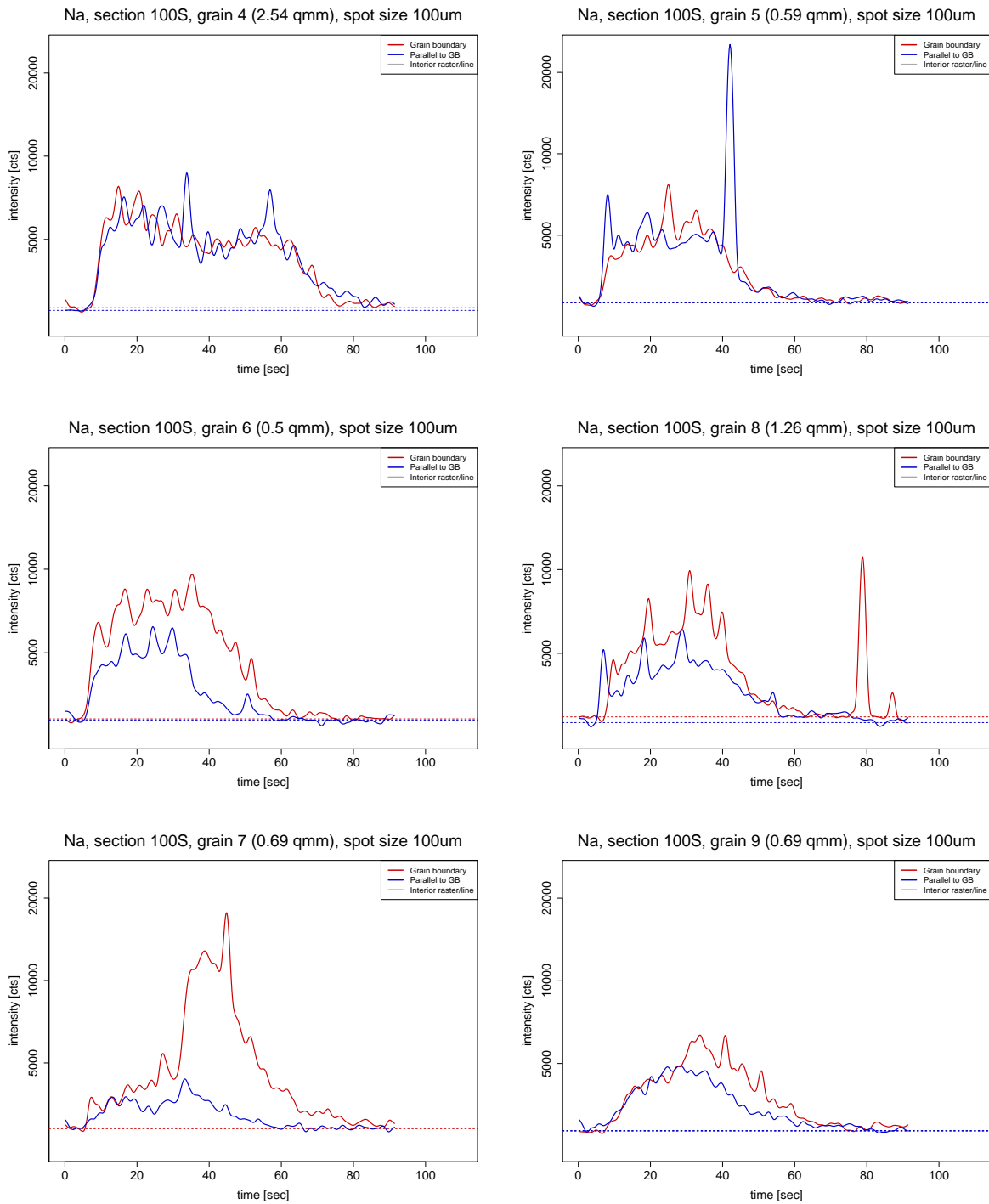


Figure 38: Even the deepest small grain section shows a difference in impurity content for four out of six grains. Single large peaks as in the parallel line signal for grain 5 could be interpreted as a particle response. Grain 1 to 3 from this section were left out as there is no signal above background level.

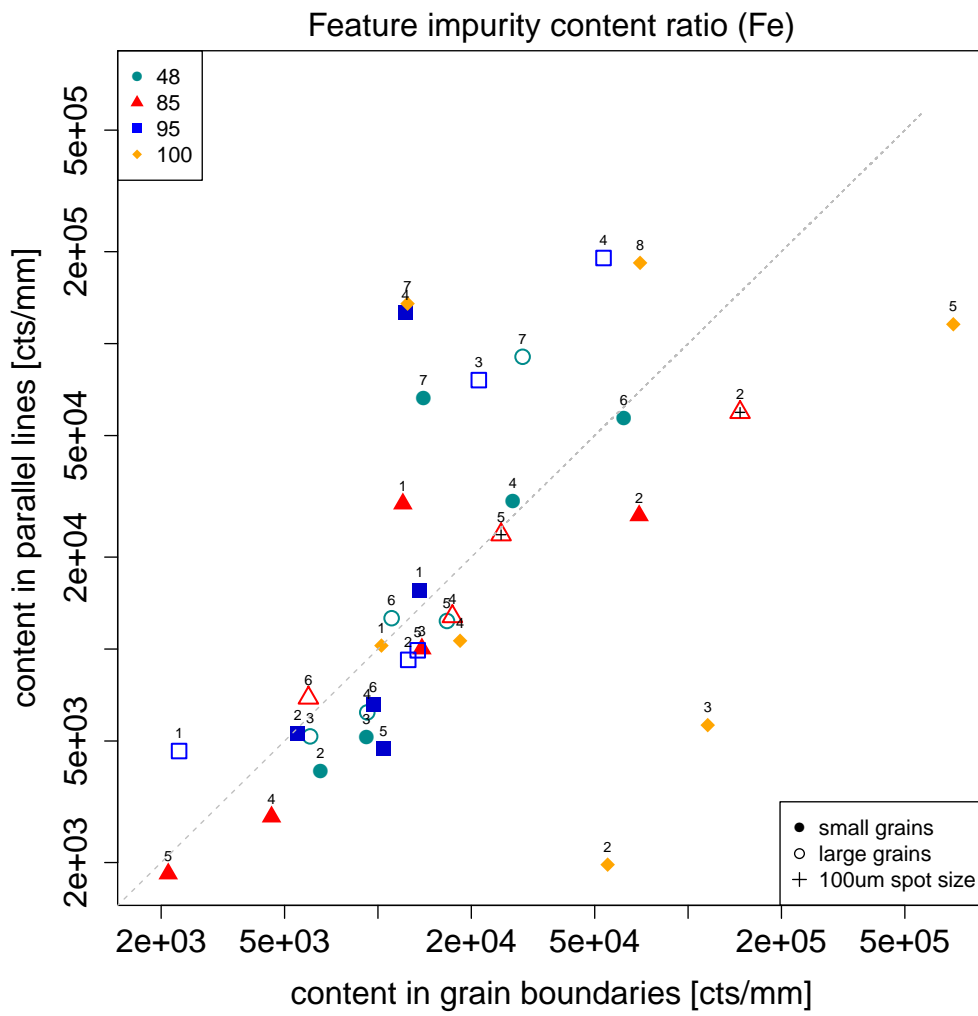


Figure 39: Same fig. as fig. 21 with grain numbers indicated.

C.2 Iron

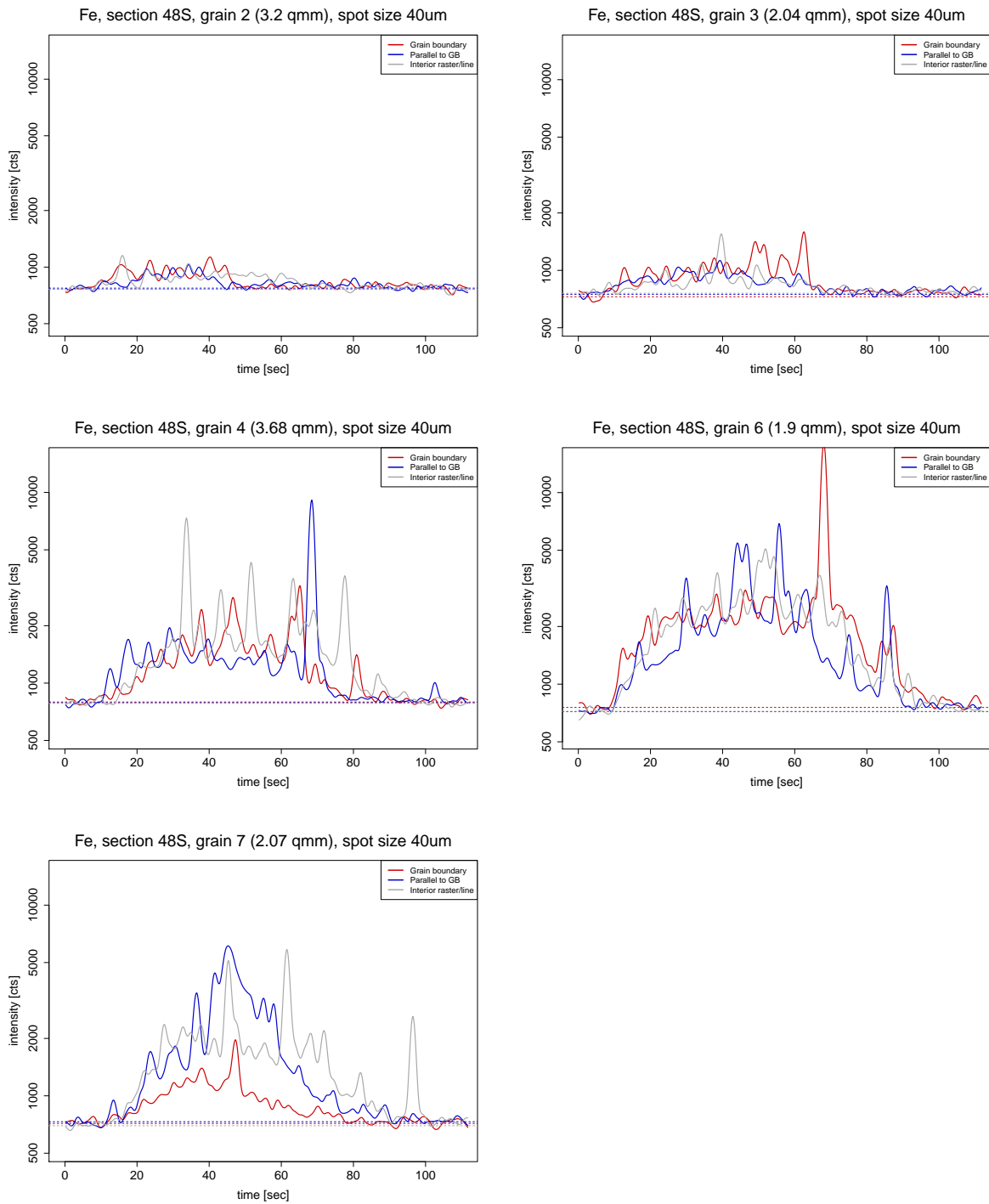


Figure 40: The data shows different characteristics between grains. Large peaks occur in all features, noticeably in the grain interiors.

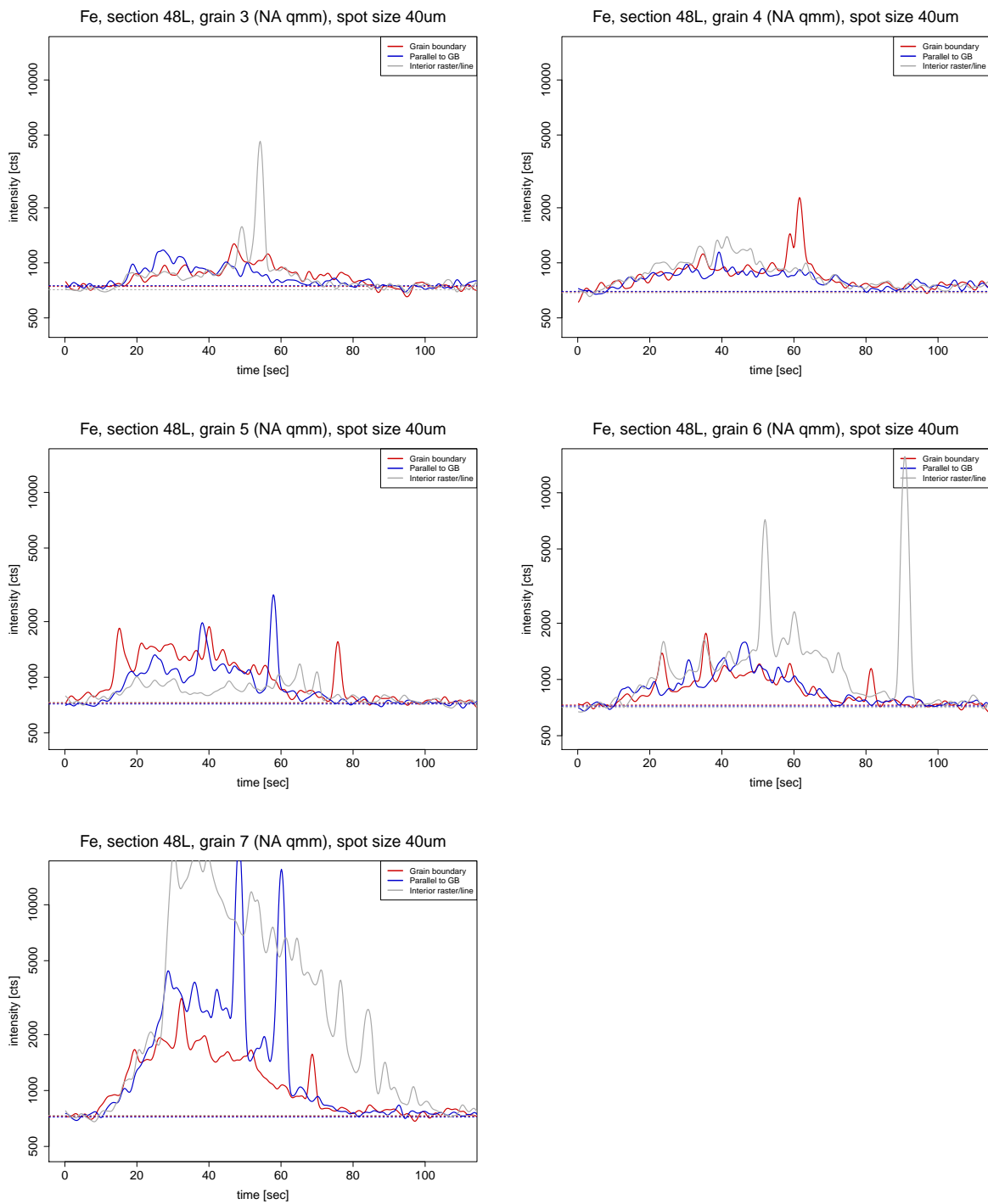


Figure 41: Three out of four grains are showing peaks in the grain interior.

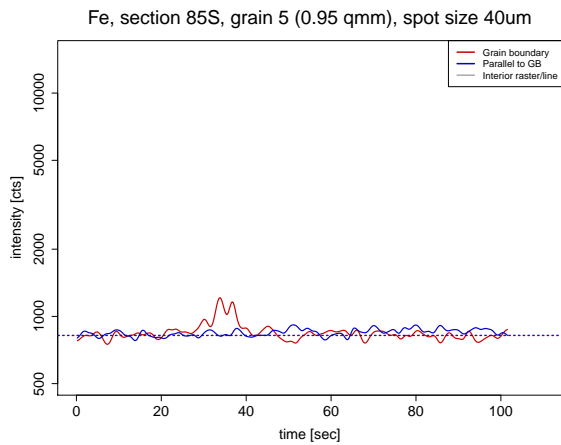
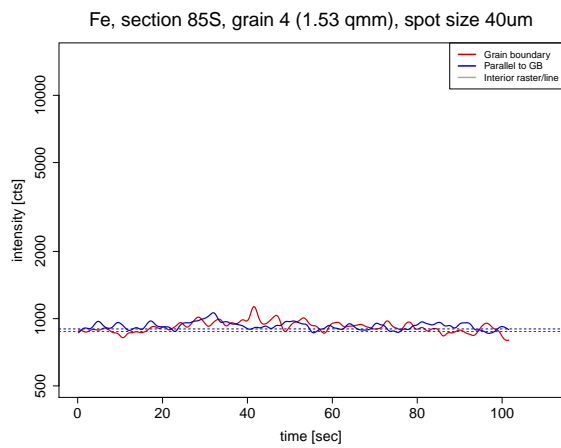
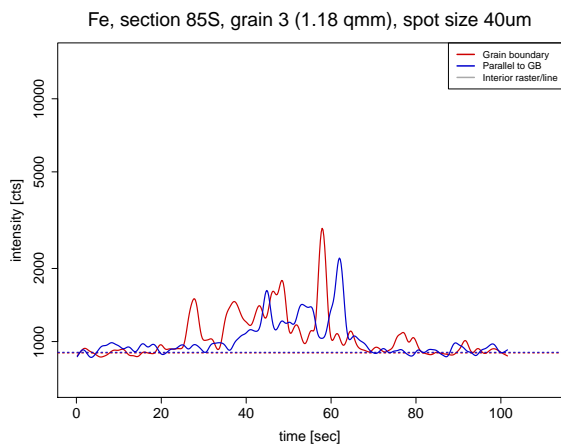
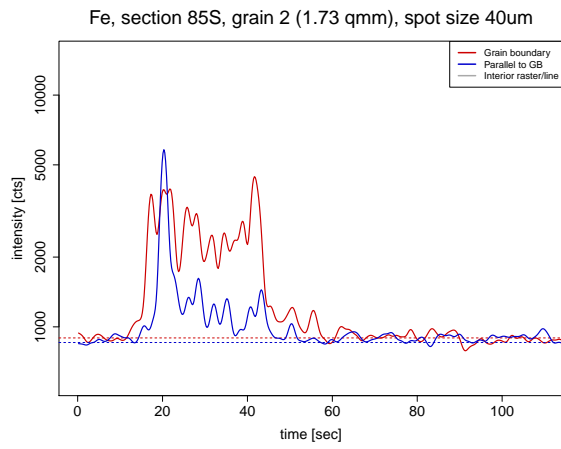
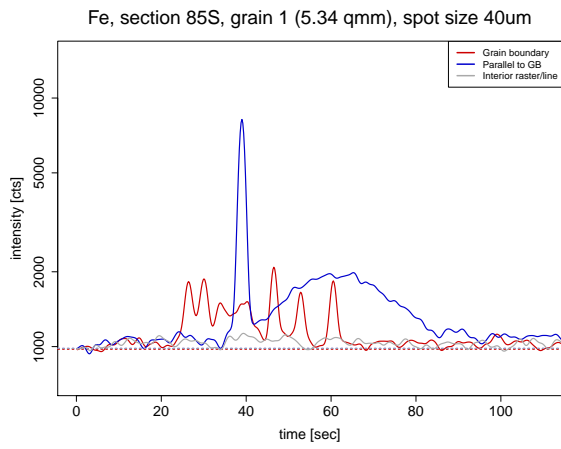


Figure 42: Smoothed data for iron.

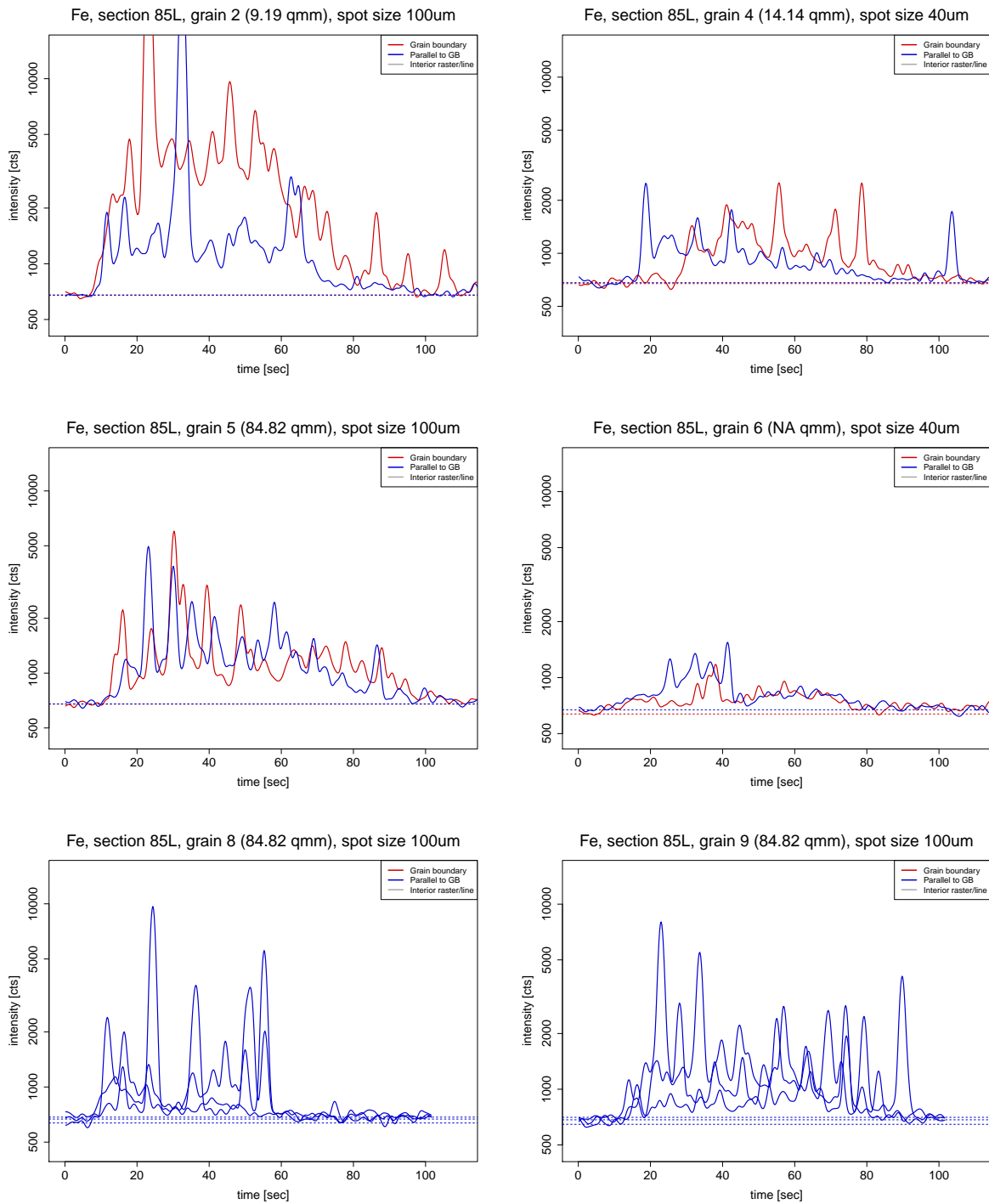


Figure 43: Grain 2 is a rare example of iron-enriched grain boundary. Grain “8” and “9” show three parallel lines from different parts of the grain boundary of the very large grain (5), illustrating the variability of the signal on the 200 um-scale.

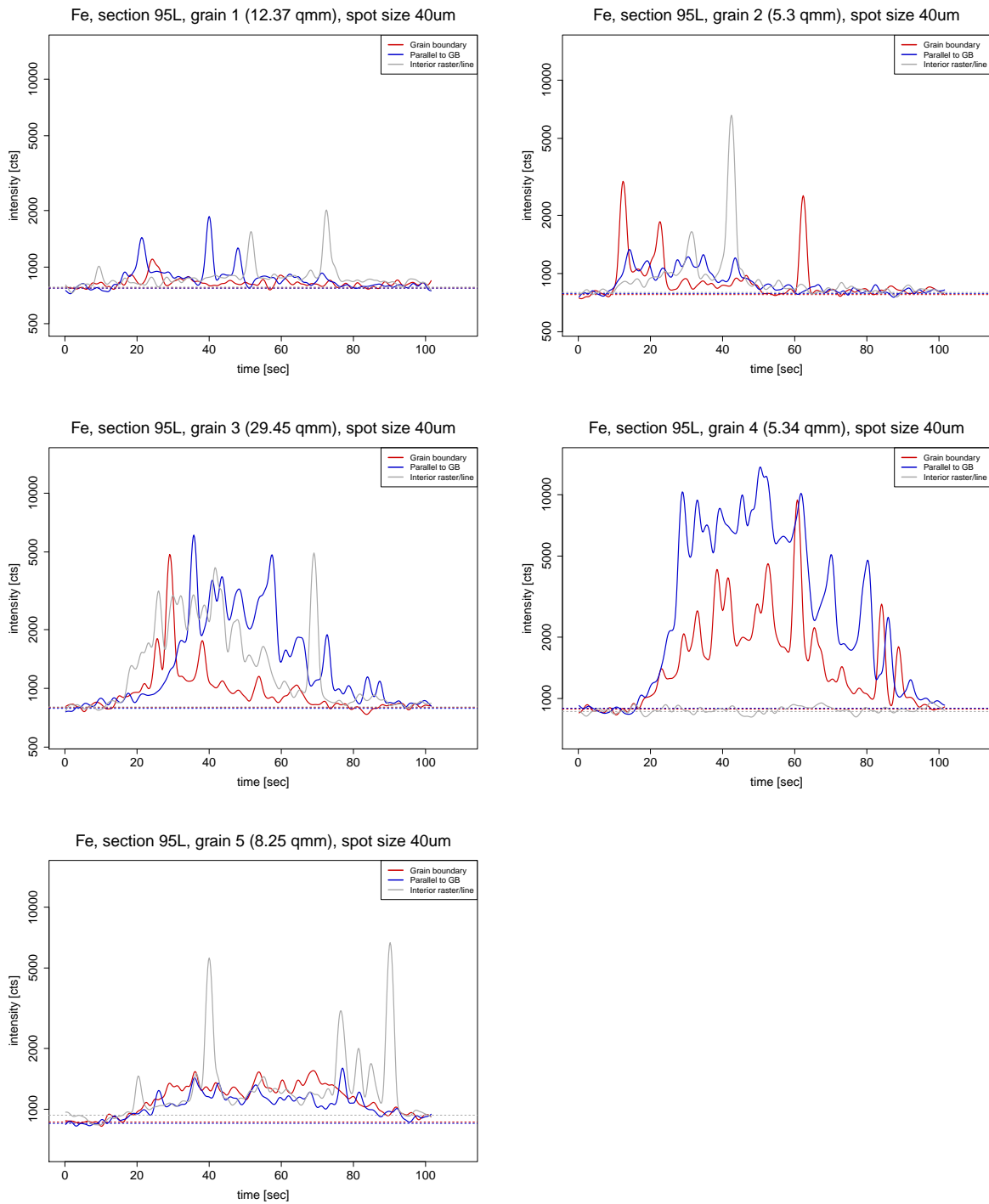


Figure 44: Two grains have higher content parallel to the grain boundary, two grains are dominated by peaks.

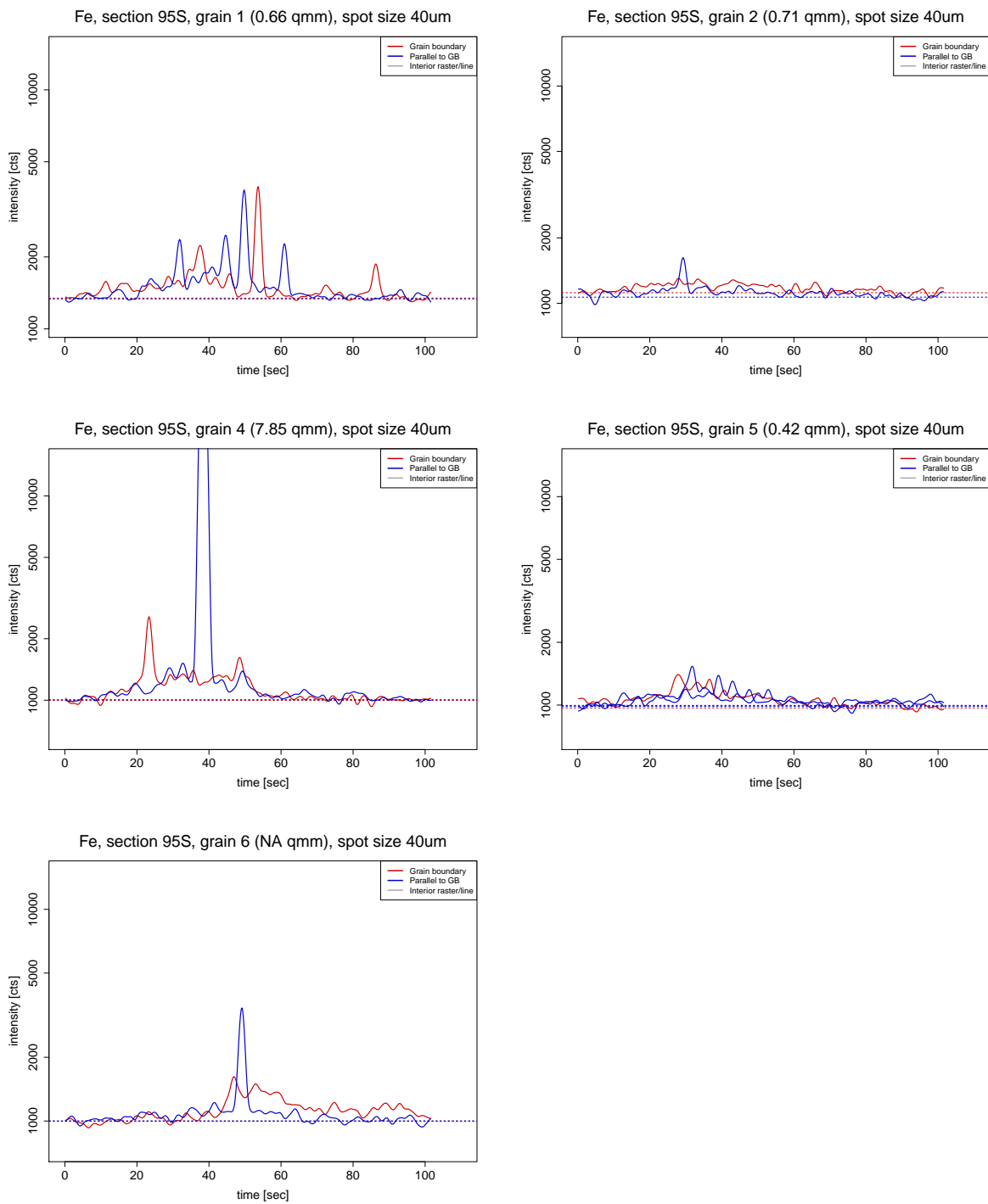


Figure 45: Like 85S this small grain section produces little signal, besides the occasional peak.

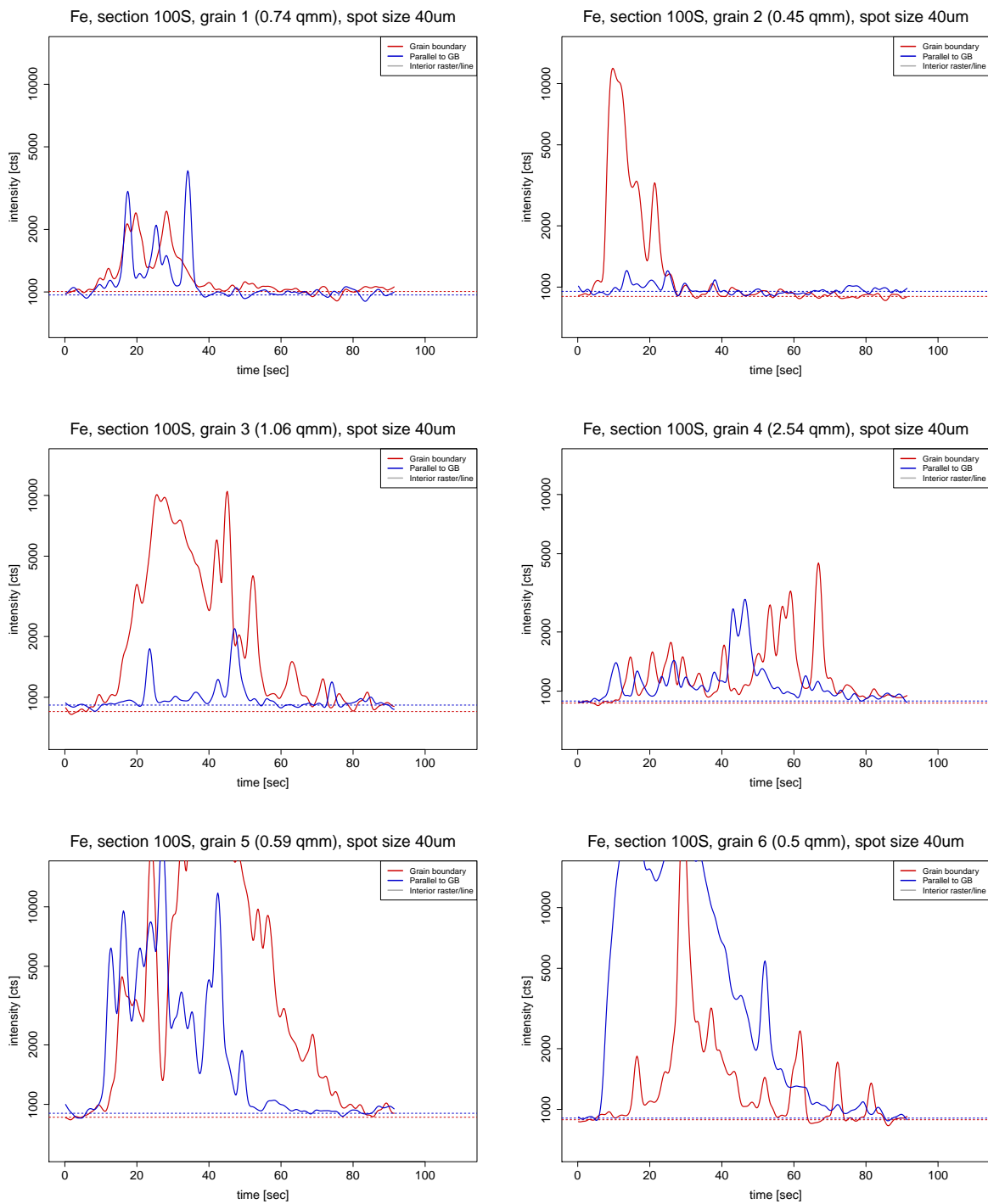


Figure 46: Overall iron content is larger than in any other section. Three grains have clearly iron-enriched grain boundaries, three grains have clearly iron-enriched parallel lines, two grains are nondescript. The data shows many peaks.

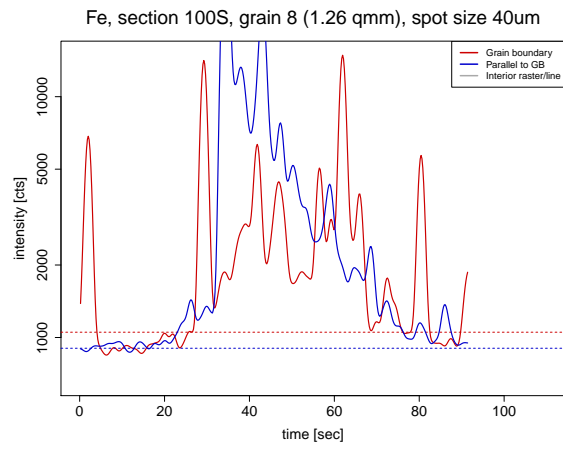
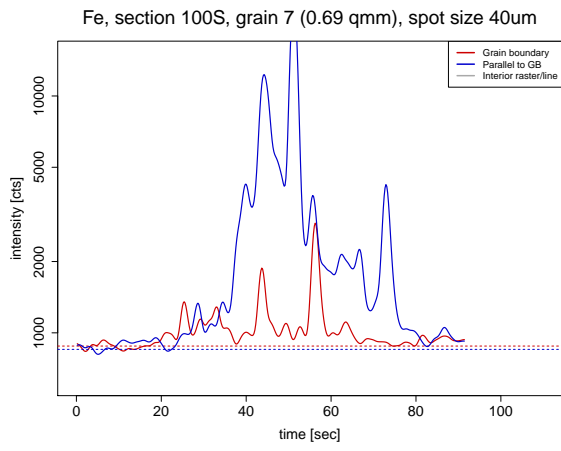


Figure 47: 100S continued.